

1 **Impacts of lake on diurnal evolution of surface PM_{2.5} concentrations**
2 **around a typical megacity of China**

3 Zining Yang¹, Qike Yang^{1*}, Chun Zhao^{1,2,3,4}, Zihan Xia¹, Qiuyan Du¹, Gudongze Li¹,
4 Mingyue Xu¹, Zhiyuan Hu^{5,6,7}, Renmin Yuan¹, Jiawang Feng¹, Jun Gu¹, and Yubin Li⁸

5 ¹National Key Laboratory of Deep Space Exploration/Joint Laboratory of Fengyun
6 Remote Sensing, School of Earth and Space Sciences, University of Science and
7 Technology of China, Hefei, China

8 ²State Key Laboratory of Fire Science, University of Science and Technology of China,
9 Hefei, China

10 ³Institute of Frontier and Interdisciplinary Research in High-Performance Computing
11 Systems and Software, University of Science and Technology of China, Hefei, China

12 ⁴Laoshan Laboratory, Qingdao, China

13 ⁵College of Atmospheric Science, Lanzhou University, Lanzhou, 730000, China

14 ⁶Collaborative Innovation Center for West Ecological Safety (CIWES), Lanzhou
15 University, Lanzhou 730000, China

16 ⁷Southern Marine Science and Engineering Guangdong Laboratory (Zhuhai)

17 ⁸School of Atmospheric Physics, Nanjing University of Information Science and
18 Technology, Nanjing, China

19

20 *Corresponding author: Qike Yang (yangqike@ustc.edu.cn)

21

22 **Key Points:**

23 1. Lake-land thermal contrasts drive a diurnal reversal in air quality by facilitating
24 daytime accumulation while promoting nighttime urban dispersion.

25 2. Daytime PM_{2.5} increase is dominated by secondary PM_{2.5} formation, while nighttime
26 purification results from enhanced vertical mixing of primary PM_{2.5}.

27 3. Suppressed boundary layers, weak mixing, and low deposition create lake “storage
28 zones,” while breeze-driven convergence intensifies shoreline pollution.

29

30 **Abstract**

31 Lake-land thermal contrasts significantly modulate regional air quality, yet the
32 coupling mechanisms by which inland lakes regulate the diurnal evolution of PM_{2.5} and
33 its components remain poorly understood. This study conducts high-resolution (1 km)
34 WRF-Chem simulations over Lake Chaohu and the adjacent megacity of Hefei, China,
35 during spring to elucidate these interactions. Results reveal a distinct diurnal reversal
36 effect. During daytime, the lake presence facilitates PM_{2.5} increases of predominantly
37 0-10 ug/m³ both over the lake and in surrounding urban areas by suppressed planetary
38 boundary layer height, weakened vertical mixing, and reduced dry deposition velocities,
39 which collectively transform the lake into “storage zone” that prolongs PM_{2.5} lifetimes.
40 This accumulation is dominated by secondary PM_{2.5}, as the cooler and more humid lake
41 air thermodynamically favors the ammonium nitrate formation. Furthermore,
42 convergence zones where lake breezes meet background winds create localized
43 stagnation traps that intensify shoreline pollution. At night, while the lake surface
44 maintains higher PM_{2.5} concentrations than surrounding land, its impact on the city
45 reverses, exerting a purification effect with urban PM_{2.5} decreasing by predominantly
46 0-10 μg/m³ as land-breeze circulation enhances vertical mixing and facilitates primary
47 pollutant dispersion. Sensitivity experiments reveal that failing to distinguish lake
48 surfaces in emission inventories can significantly amplify daytime pollution. These
49 findings emphasize that lakes act as complex dual regulators of urban air quality, with
50 identified mechanisms likely applicable to other urban-lake systems globally. This
51 study highlights the necessity of high-resolution meteorological modeling and precise
52 surface characterization for improved air quality forecasting in lake-adjacent
53 megacities regions.

54

55

56

57

58 **1. Introduction**

59 Rapid urbanization and economic development in China over recent decades
60 have led to severe urban air pollution (e.g., Lei et al., 2011; Li et al., 2011; Liu et al.,
61 2018). Fine particulate matter (PM), known as PM_{2.5} (particulate matter with
62 aerodynamic diameters less than 2.5 μm), is the primary air pollutant (e.g., Zhang et al.,
63 2012; Hu et al., 2014a; Chai et al., 2014; Wang et al., 2014; He et al., 2017; Lu et al.,
64 2017). Ambient PM_{2.5} poses significant health risks including lung cancer, ischemic
65 heart disease, and respiratory disorders (e.g., Hu et al., 2014b; Guo et al., 2017; Ho et
66 al., 2018; Yang et al., 2019; Chen and Hoek, 2020; Yue et al., 2021), while also affecting
67 visibility (Li et al., 2014), radiation budget (Steiner et al., 2013), atmospheric
68 circulation (Jiang et al., 2017), cloud properties (Unger et al., 2009), and regional
69 climates (Guo et al., 2016; Li et al., 2016; Li et al., 2017c). The formation and evolution
70 of urban PM_{2.5} are comprehensively influenced by source emissions, long-range
71 transport, chemical transformations, and meteorological conditions (Guo et al., 2014;
72 Huang et al., 2014; Zhang et al., 2015b; Zhang et al., 2013; Hu et al., 2014c; Miao et
73 al., 2017; Miao et al., 2013; Zhang et al., 2015a). Among these factors, local-scale
74 underlying surface characteristics, such as land use type and surface cover, exert crucial
75 influence on PM_{2.5} distributions by altering surface energy balance, water cycles, and
76 momentum exchange, which subsequently affects turbulent mixing, pollutant transport,
77 deposition, and chemical processes.

78 Lakes exert a significant “lake effect” on surrounding areas through their
79 distinctive physical properties. Their high heat capacity, low albedo, and substantial
80 moisture supply create thermal contrasts with surrounding terrestrial surfaces,
81 modifying local and regional weather and climate patterns (Levy et al., 2010; Hayden
82 et al., 2011; Wentworth et al., 2015). Differential heating drives the formation of local
83 circulation systems. During daytime, solar heating warms land surfaces while
84 minimally affecting water, creating temperature gradients that generate pressure
85 gradients and initiate lake breezes (Atkinson, 1981; Stull, 1988). Air above the lake
86 moves inland in a shallow inflow layer while air aloft over land returns offshore. As

87 cooler lake air advances over warmer land surfaces, it forms a thermal internal
88 boundary layer (TIBL) that increases in height with inland distance (Lyons and Olsson,
89 1973; Garratt, 1990). At the leading edge of the lake breeze, air is forced upward at the
90 convergence zone (lake-breeze front) where cooler lake air meets warmer inland air,
91 producing enhanced vertical motion, increased moisture and wind shear, decreased
92 temperature, and directional wind shifts (Lyons, 1972). At night, the temperature
93 gradient reverses, generating a land breeze.

94 Lakes can significantly impact the atmospheric environment. Research on lake-
95 induced local circulation has been extensively conducted worldwide, predominantly
96 focusing on lake effects on ozone formation and distribution. Nocturnal stable boundary
97 layers and land breezes cause substantial accumulation of ozone and its precursors over
98 lake surfaces, resulting in significant ozone concentration increases after sunrise (Capps
99 et al., 2010; Fast and Heilman, 2005). Dye et al. (1995) demonstrated that temperature
100 inversions over Lake Michigan confine urban pollution over the lake, where other
101 emissions may be located within or above this inversion layer but experience limited
102 vertical mixing. Additionally, lake breezes transport ozone downwind during daytime.
103 Ozone moves landward via airflow and disperses upward under the influence of
104 updrafts at the lake breeze front (Lyons et al., 1995; Wentworth et al., 2015). Due to
105 downdrafts from the backflow effect, high ozone concentrations can be detected in mid-
106 lake regions (Burley et al., 2015; Hayden et al., 2011). Some pollutants may re-enter
107 the onshore airflow and spiral along the lake shoreline (Makar et al., 2010; Harris and
108 Kotamarthi, 2005). Levy et al. (2010) observed high O₃ concentrations over the
109 southern Great Lakes, where daytime updrafts transport O₃ to higher altitudes over
110 urban areas, while downdrafts subsequently transport O₃ back to the lake surface.
111 Furthermore, lake-breeze circulations can influence pollution transport by trapping
112 pollutants within the shallow TIBL (Sills et al., 2011), and the complex wind patterns
113 induced by lakes can cause rapid spatial variations in pollutant concentrations over
114 small distances (Hayden et al., 2011; Levy et al., 2008). Wang et al. (2023) found ozone
115 concentration in lakeshore areas within 5 km of Lake Taihu approximately 20 ppb
116 higher than other regions due to TIBL formation and lake-breeze regulation.

117 In addition to generating local circulation through thermal differences between
118 lakes and land surfaces, lakes also influence O₃ concentrations through modifications
119 to other critical meteorological conditions. Lakes can reduce air temperature and
120 planetary boundary layer height (PBLH) (Wang et al., 2017; Zhang et al., 2017) while
121 altering the spatial distribution of pollutant precursors (Hu and Xue, 2016; Li et al.,
122 2019), affecting both the diffusion of air pollutants and reaction conditions for
123 secondary pollutant formation, potentially causing ozone pollution in surrounding
124 urban areas. Furthermore, dry deposition rates of O₃ over water surfaces are
125 substantially lower compared to terrestrial surfaces (Monks et al., 2015), allowing O₃
126 to accumulate within the shallow boundary layer above the lake surface (Brook et al.,
127 2013). This reduced deposition efficiency contributes to the persistence and buildup of
128 ozone concentrations over lake areas, which can subsequently be transported to
129 adjacent regions through lake-breeze circulation patterns.

130 In contrast to the extensive literature on ozone, limited research has examined the
131 complex influence of lake effects on PM_{2.5}. Existing studies have primarily identified
132 that the vertical and horizontal motions within lake breeze circulation systems cause
133 the re-circulation of primary and secondary pollutants (Brook et al., 2013; Harris and
134 Kotamarthi, 2005) and enhance aerosol formation rates compared to the background
135 conditions (Brook et al., 2013; Hayden et al., 2011). For instance, increased
136 concentrations of secondary pollutants, such as sulfate and nitrate, have been observed
137 following lake breeze circulation events (Fosco and Schmeling, 2006). Despite these
138 findings, significant knowledge gaps remain. Existing studies have primarily focused
139 on individual processes or specific pollution episodes, lacking systematic investigation
140 into how lakes affect the spatial distribution and diurnal variation of PM_{2.5} and its
141 different components. Furthermore, the complex interactions among lake-related
142 processes, including local circulation, boundary layer mixing, dry deposition, and
143 chemical transformation, and how these processes collectively shape PM_{2.5} distribution
144 remain poorly understood. Moreover, existing research has been largely concentrated
145 in the North American Great Lakes region, while lake-urban interactions in rapidly
146 urbanizing areas characterized by intensive anthropogenic emissions, particularly in

147 East Asia, remain underexplored.

148 In summary, these research gaps highlight the need for systematic investigation
149 of lake effects on PM_{2.5} pollution. Existing studies lack systematic investigation into
150 how lakes affect the spatial distribution and diurnal variation of PM_{2.5} and its
151 components (primary and secondary aerosols) within lake-urban systems. Moreover,
152 how lake-related processes such as local circulation, boundary layer mixing, dry
153 deposition, and chemical transformation interact and collectively influence pollutant
154 concentrations remains poorly understood (Hayden et al., 2011; Zhang et al., 2017;
155 Wang et al., 2023). Lake Chaohu, one of China's five major freshwater lakes, provides
156 an ideal case for addressing these gaps. The megacity of Hefei, adjacent to the lake's
157 northern shore, forms a typical lake-urban system exemplifying the common global
158 pattern where large cities border natural water bodies (Chen et al., 2017; Peng et al.,
159 2019; Hu and Li, 2020). Rapid industrialization and urbanization in this region have
160 led to severe air pollution, yet the complex interactions between substantial urban
161 emissions and lake-induced meteorological effects remain underexplored. Therefore,
162 this study conducts high-resolution (1 km) WRF-Chem simulations during a spring
163 pollution episode (March 2019) with comparative scenarios including (Lake) and
164 excluding (Nolake) the lake to systematically investigate how lake effects influence the
165 spatiotemporal distribution of PM_{2.5} and its key components, and to elucidate the
166 coupling mechanisms between physical processes (turbulent mixing, dry deposition,
167 local circulation) and chemical processes. It should be emphasized that this sensitivity
168 experiment approach is employed as a scientific tool to isolate and quantify the lake's
169 influence on PM_{2.5} distributions, rather than to evaluate the feasibility of lake removal
170 as an air quality management strategy. The primary objective is to advance our
171 mechanistic understanding of how large water bodies affect atmospheric pollution in
172 megacity environments. The findings will provide scientific support for air quality
173 forecasting and pollution control strategies in lake-adjacent cities.

174 The paper is organized as follows: Section 2 introduces the WRF-Chem model
175 configuration, the design of different experiments, and emissions from different sources.
176 Section 3 presents the spatial distribution and diurnal variation of PM_{2.5} concentrations

177 from different sensitivity experiments and reveals the key mechanisms of lake effect on
178 the PM_{2.5}. Section 4 present the conclusion and discussion of the analysis.

179

180 **2. Methodology**

181 **2.1 WRF-Chem**

182 In this study, the version of WRF-Chem updated by the University of Science
183 and Technology of China (USTC version of WRF-Chem) is used. Compared with the
184 publicly released version, this USTC version of WRF-Chem includes some additional
185 functions such as the diagnosis of radiative forcing of aerosol species, land surface
186 coupled biogenic VOC (volatile organic compound) emission, aerosol-snow interaction,
187 improved PBL mixing of aerosols, and a detailed diagnosis of the contributions of each
188 crucial process to pollutant concentrations (Zhao et al., 2013a; Zhao et al., 2013b; Zhao
189 et al., 2014; Zhao et al., 2016; Hu et al., 2019; Du et al., 2020; Zhang et al., 2021; Yang
190 et al., 2025).

191 The configuration of WRF-Chem in this study is given in Table 1. In summary,
192 the Model for Simulating Aerosol Interactions and Chemistry (MOSAIC) and the
193 CBM-Z (carbon bond mechanism) photochemical mechanism (Zaveri and Peters, 1999)
194 are used. The MOSAIC aerosol scheme includes important physical and chemical
195 processes such as nucleation, condensation, coagulation, aqueous-phase chemistry, and
196 water uptake by aerosols. Sulfate (SO₄²⁻), nitrate, (NO₃⁻), ammonium (NH₄⁺), sea salt,
197 mineral dust, organic matter (OM), black carbon (BC), and other (unspecified)
198 inorganics (OIN) constitute the prognostic species in MOSAIC. OIN represents the
199 unidentified aerosol species other than OM, BC, sulfate, ammonium, and nitrate in
200 emissions if any, which are composed mostly of minerals in emissions in this study.
201 The aerosol direct effect is coupled to the Rapid Radiative Transfer Model (RRTMG)
202 (Mlawer et al., 1997; Iacono et al., 2000) for both SW (shortwave) and LW (longwave)
203 radiation as implemented by Zhao et al. (2011). The optical properties and direct
204 radiative forcing of individual aerosol species in the atmosphere are diagnosed
205 following the methodology described in Zhao et al. (2013b). We also turned on the

206 aerosol indirect effect, which represents the interactions between aerosols and clouds,
207 including the first and second indirect effects, activation/resuspension, wet scavenging,
208 and aqueous chemistry (Gustafson et al., 2007; Chapman et al., 2009). The photolysis
209 rate is computed by the Fast-J radiation parameterization (Wild et al., 2000). Dry
210 deposition of aerosol mass and number is simulated following the approach of
211 Binkowski and Shankar (1995), which includes both particle diffusion and gravitational
212 effects. Other model configurations include the Yonsei University (YSU) nonlocal PBL
213 parameterization scheme (Hong et al., 2006), the Noah land surface model (Chen and
214 Dudhia, 2001) for the surface layer process, and the Morrison two-moment scheme
215 (Morrison et al., 2009) for cloud microphysics.

216

217 **2.2 Numerical experiments**

218 The study period spans from 5 to 20 March 2019. Following previous research
219 (Yang et al., 2025), the first 5 day are considered to be the model spin-up time, while
220 the remaining integration period (10-20 March 2019) is used for analysis. The selected
221 episode was strategically chosen based on several considerations. This period
222 corresponds to the pollution season when PM_{2.5} concentrations are typically much
223 higher than in summer, and lake-land thermal contrasts remain sufficiently strong to
224 drive significant lake-breeze circulations. Importantly, the episode was characterized
225 by predominantly clear-sky conditions, with total column cloud water and cloud ice
226 content remaining at low levels (less than 0.1 kg/m² in most areas) and negligible
227 precipitation (hourly accumulation greater than 0.5 mm). These conditions are
228 favorable for isolating the intrinsic lake effects while minimizing confounding
229 influences from cloud microphysics and wet scavenging on PM_{2.5} distributions
230 (detailed spatial distributions are not shown here). Additionally, March represents a
231 transitional season between winter and summer circulation patterns, which facilitates
232 the investigation of interactions among lake-induced meteorological perturbations,
233 boundary layer evolution, and PM_{2.5} pollution. Given the extremely high computational
234 cost of 1-km resolution WRF-Chem simulations, the 10-day period can capture diurnal
235 variations of lake effects while remaining computationally feasible. It should be noted

236 that ERA5 reanalysis dataset (<https://rda.ucar.edu/datasets/ds630.0/>, last access: 15
237 April 2019) indicates significant differences in large-scale circulation across different
238 months during the pollution season (October, January, March) (see Figure S1 in
239 Supporting Information), and the selected period represents springtime transitional
240 conditions with moderate background winds. Therefore, our results should be
241 interpreted as lake effects under specific springtime meteorological conditions, and the
242 lake impact mechanisms may differ in other seasons, rather than being statistically
243 representative of all pollution seasons. The sensitivity experiments employ identical
244 initial and boundary conditions, ensuring that simulation differences primarily reflect
245 perturbations induced by lake presence.

246 As shown in Figure 1a, a three-domain nested simulation is implemented with
247 spatial resolutions of 25, 5, and 1 km resolution, respectively. The outermost domain
248 encompasses East, North, and South China with 140 x 105 grid cells (107°-128°E, 17°-
249 45°N) at 25 km horizontal resolution. The intermediate domain covers the Yangtze
250 River Delta (YRD) region in East China, consisting of 250 x 250 grid cells (111.8°-
251 121.8°E, 27°-37°N) at 5 km resolution. The innermost domain centers on Hefei City
252 and encompasses Chaohu Lake, covering 150 x 150 grid cells (116.6°-117.8°E, 31.2°-
253 32.4°N) at 1 km horizontal resolution. Domain 3 was selected as the main scope of
254 study for this research, as shown in Figure 1b. Hefei, the capital city of Anhui province
255 and a typical megacity in the YRD, is located in the mid-latitude zone with a humid
256 subtropical monsoon climate. The solid black triangle indicates the location of Hefei,
257 as shown in Figure 1b. Chaohu Lake (31.40°-31.72°N, 117.27°-117.85°E), China's
258 fifth-largest freshwater lake, is situated in central Anhui Province, approximately 15
259 km southeast of Hefei. The lake encompasses approximately 780 km² with an average
260 depth of 3 m and a 176 km shoreline. Thus, in this study, the lake is characterized as a
261 large, shallow, freshwater body situated within an inland monsoon region, a
262 configuration representative of numerous lakes in East Asia. We define lake impact as
263 the aggregate atmospheric perturbation driven by the thermal and physical contrasts
264 between the water surface and the surrounding terrestrial landscape. This includes the
265 modification of the surface energy balance, alterations in aerodynamic roughness, and

266 the regulation of atmospheric moisture, which collectively govern the development of
267 the internal boundary layer and the thermodynamic stability of the overlying air.
268 Specifically, this is expressed as the difference between the Lake (control) and Nolake
269 (sensitivity) experiments, or between the Lake_emis (control) and Nolake_emis
270 (sensitivity) experiments, as discussed below. This approach allows us to isolate the net
271 effect of the intrinsic physical and chemical properties of the lake on the overlying
272 atmosphere, providing a clear mathematical framework to evaluate how the presence
273 of the water body modulates the regional environment.

274 We derive terrain information from a high-resolution (~ 1 km) US Geological
275 Survey (USGS) topographic data and interpolate it onto the WRF grid. Furthermore, to
276 better resolve the PBL structure and mixing processes, we implemented a finer vertical
277 resolution within the PBL. A total of 50 terrain-following vertical eta-layers extending
278 from the surface to approximately 15 km were used, with 30 layers distributed below 2
279 km above the ground to describe the atmospheric boundary structure in detail. The
280 vertical layer was strategically designed with 7 layers below 200 meters (each
281 approximately 20 meters in height), 3 layers between 200 and 300 meters (each about
282 30 meters in height), and 8 layers between 300 and 1000 meters (each approximately
283 80 meters in height). This configuration comprehensively captures mixed layer
284 development and key turbulent processes (e.g., entrainment and surface flux exchange)
285 through layer densification, which is sufficient to capture PBL turbulent mixing.

286 Additionally, to ensure consistent boundary forcing across the three nested
287 domains, initial and boundary conditions are configured hierarchically. For the 25 km
288 resolution domain, meteorological initial and lateral boundary conditions are obtained
289 from the National Center for Environmental Prediction (NCEP) Final Reanalysis (FNL)
290 data at $1^\circ \times 1^\circ$ resolution and 6 h temporal intervals. Initial and boundary conditions for
291 the trace gases and aerosol species are provided by the quasi-global WRF-Chem
292 simulation with 360×145 grid cells (67.5°S - 77.5°N , 180°W - 180°E) at $1^\circ \times 1^\circ$
293 resolution. More details about the quasi-global WRF-Chem simulation can be found in
294 Zhao et al. (2013b). The 5 km resolution simulation obtains its initial and boundary
295 conditions from the 25 km simulation output, while the 1 km resolution simulation is

296 similarly driven by the 5 km simulation results. Furthermore, the 25 km resolution
297 simulation turns on the option of cumulus parameterization, which uses the Kain-
298 Fritsch cumulus and shallow convection scheme (Kain, 2004) to simulate sub-grid scale
299 clouds and precipitation. However, this option is turned off in the other two higher-
300 resolution simulations because the fine-resolution is sufficient to resolve the cloud-
301 forming processes.

302 The land cover dataset is derived from a 1 km horizontal resolution dataset for
303 China (Zhang et al., 2021). The land use categories follow the United States Geological
304 Survey's (USGS) 24-category classification, and the dataset is based on China's land
305 cover conditions as of 2015. This provides a more accurate representation of current
306 land cover, particularly for eastern China, which has experienced intensive urban
307 expansion since the 2000s. Figure 2a shows the land cover data at 1 km resolution, with
308 detailed descriptions of the legend and land cover classes provided in Table S1 in the
309 Supplement. This set of simulations is referred to as the "Lake experiment". To evaluate
310 the impact of lake effects on meteorological conditions and PM_{2.5} concentrations in
311 surrounding urban regions, we conducted a sensitivity experiment in which Chaohu
312 Lake was replaced with cropland, the dominant land use type surrounding the lake, as
313 illustrated in Figure 2b. This experiment is referred to as the "Nolake experiment".
314 Specifically, only the lake area was replaced with cropland while preserving land-use
315 types in other regions, with all other conditions remaining unchanged, including initial
316 and boundary conditions, emissions, and parameterization schemes. With the exception
317 of part of Section 3.3, all other analyses in this study are based on the results of these
318 two comparative experiments.

319

320 **2.3 Emissions**

321 Conventionally, lake surfaces are regarded as emission-free areas, with
322 theoretical emission rates assumed to be zero. However, due to the coarse spatial
323 resolution of current emission inventories, most datasets cannot effectively distinguish
324 between land and lake surfaces. When emission inventories are spatially allocated or
325 downscaled to finer grid resolutions for air quality modeling, the lack of explicit lake-

326 land differentiation in these inventories results in emission fluxes being distributed
327 uniformly across grid cells, thereby erroneously assigning anthropogenic emissions to
328 lake areas that should theoretically be emission-free. Consequently, anthropogenic
329 emissions are often assigned to lake regions in many previous studies, which may
330 introduce biases and limit our understanding of atmospheric processes over lake
331 environments. To address the differences between scenarios with and without actual
332 emissions over the lake surface, this study designed four sets of comparative
333 experiments. The first two experiments are the previously mentioned “Lake experiment”
334 and “Nolake experiment”, in which lake surface emissions were masked (i.e., set to
335 zero), allowing investigation of how an emission-free lake surface affects the
336 distribution of particulate matter in the lake region and adjacent urban areas. The results
337 presented in Sections 3.1 and 3.2 are based on these two experiments. Additionally, to
338 assess scenarios where emissions are retained over the lake surface, a prevalent
339 configuration in current air quality modeling studies due to emission inventory
340 limitations, two additional experiments, “Lake_emis experiment” and “Nolake_emis
341 experiment”, were conducted. These experiments preserve the original lake emissions
342 while all other model settings remain consistent with the “Lake experiment” and
343 “Nolake experiment”. The purpose of these additional experiments is to evaluate how
344 the erroneous assignment of emissions to lake surfaces, a systematic bias resulting from
345 insufficient spatial resolution in emission inventories, may alter the lake effects
346 revealed in the idealized zero-emission scenarios and subsequently impact PM_{2.5}
347 distribution patterns in surrounding urban areas. Related analyses are presented in
348 Section 3.3. This four comprehensive experimental design enables systematic
349 evaluation of how both the presence of lake surfaces and the configuration of lake
350 emissions influence regional air pollution and lake-urban interactions.

351 For all simulations, anthropogenic emissions for the outer quasi-global
352 simulation are derived from the Hemispheric Transport of Air Pollution version-2
353 (HTAPv2) at 0.1° x 0.1° horizontal resolution with monthly temporal resolution for
354 2010 (Janssens-Maenhout et al., 2015). The Multi-resolution Emission Inventory for
355 China (MEIC) at 0.25° x 0.25° horizontal resolution for 2019 (Li et al., 2017a; Li et al.,

2017b; Zheng et al., 2018; Geng et al., 2024a) is used to replace emissions over China within the simulation domain. Specially, anthropogenic emissions for Domain 1 (D1) are obtained from the original HTAPv2 and MEIC inventory interpolated to 25 km resolution. Emissions for Domain 2 (D2) and Domain 3 (D3) are subsequently derived by interpolating the 25 km resolution emissions to 5 km and 1 km resolution domains, respectively. This study primarily focuses on PM_{2.5}. The spatial distribution of PM_{2.5} emissions averaged over the entire day for both the Lake and Nolake experiments is shown in Figure 2c, and Figure S2 illustrates the corresponding spatial distribution of PM_{2.5} emissions in both the experiments at 08:00, 11:00, 14:00, 17:00, 20:00, 23:00, 02:00, and 05:00 local time (LT) throughout the study area. Additionally, the spatial distribution of PM_{2.5} emissions in both the Lake_emis and Nolake_emis experiments averaged over the entire day is shown in Figure S3. Biomass burning emissions are obtained from the Fire Inventory from NCAR (FINN) at a 1 km horizontal resolution and 1 h temporal resolution (Wiedinmyer et al., 2011). The diurnal variation in biomass-burning emissions follows the suggestions by WRAP (2005), with injection heights based on Dentener et al. (2006) from the Aerosol Comparison between Observations and Models (AeroCom) project. Biogenic emissions were calculated using the Model of Emissions of Gases and Aerosols from Nature (MEGAN) v3.0 model (Gustafson et al., 2007; Zhang et al., 2021).

375

376 **2.4 Observational data**

377 2.4.1 Meteorological data

378 The meteorological data were obtained from automatic weather stations (AWSs),
379 which were established based on the operational standards issued by the China
380 Meteorological Administration (CMA, 2018). The hourly data underwent quality
381 control (QC) by local meteorological bureaus of Anhui, following World
382 Meteorological Organization guidelines (Estevez et al., 2011). The QC included checks
383 of consistency, such as internal, temporal-spatial, and climatic range validations. These
384 QC data were used to determine daily mean, minimum, and maximum meteorological
385 variables. The AWSs recorded various parameters, including air temperature (T, °C),

386 wind speed (U , m/s), air pressure (P , Pa), and wind direction. In this study, we focus on
387 the 3-hourly 2 m temperature and 10 m wind speed obtained from four AWS stations
388 located in the study region. The four AWS sites are marked by purple solid dots in
389 Figure 1b.

390

391 2.4.2 Environmental data

392 Ground observations of hourly $PM_{2.5}$ near-surface concentrations during March
393 2019 were obtained from the website of the Ministry of Environmental Protection of
394 China (MEP of China). As our study concentrates on the Hefei region, we selected 10
395 monitoring stations within this area for detailed analysis. These stations are marked by
396 red solid dots in Figure 1b.

397 While hourly observations for both meteorology and pollutants are available, model
398 outputs are provided at 3-hour intervals to balance computational efficiency and storage
399 requirements. Hourly output data would provide higher time resolution but significantly
400 increase storage demands. Given that we ran simulations at 1km resolution, hourly
401 outputs would have generated prohibitively large data volumes. On the other hand, this
402 3-hour output interval remains sufficient for our primary research objective of
403 investigating the diurnal reversal effect of lake impacts on $PM_{2.5}$ concentrations and
404 elucidating the coupling mechanisms between physical processes (turbulent mixing,
405 dry deposition, local circulation) and chemical processes. This approach effectively
406 captures the distinct daytime pollution enhancement and nighttime purification patterns
407 without losing essential detail for understanding lake-urban air quality interactions. To
408 ensure consistent temporal resolution between model and observations, hourly
409 observations were sampled to match our 3-hour model output intervals.

410

411 **3. Results**

412 **3.1 $PM_{2.5}$ near-surface concentrations over lake and urban areas during daytime** 413 **and nighttime**

414 Before presenting the simulation results of $PM_{2.5}$ near-surface concentrations over

415 lake and urban areas during daytime and nighttime, a systematic evaluation of the Lake
416 experiment is first conducted to verify the capability of the simulation framework in
417 reproducing real atmospheric conditions with the lake present. The evaluation covers
418 the meteorological fields and PM_{2.5} surface concentrations during the study period from
419 March 10 to 20, 2019, which are compared against in-situ observational data averaged
420 over 10 MEP sites in Hefei.

421 The model's performance in reproducing meteorological conditions is assessed by
422 comparing the simulated 10-meter wind speed and 2-meter temperature with
423 observational data from four AWSs in the Hefei region, as shown in Figure S4. Overall,
424 the model performs well in simulating both variables and successfully reproduces the
425 temporal evolution throughout the study period. The simulated 2-meter temperature
426 agrees well with observations, indicating that the model accurately characterizes the
427 surface energy budget and thermodynamic conditions that form the physical basis for
428 analyzing the lake-land thermal contrast in this study, as shown in Figure S4a. The
429 model overestimates peak wind speed during the strong wind event around March 20,
430 likely attributable to complex mesoscale interactions. Nevertheless, this bias does not
431 compromise the overall assessment of circulation characteristics throughout the study
432 period, as demonstrated in Figure S4b. The model's ability to reproduce PM_{2.5} surface
433 concentrations is then assessed against observational data from 10 MEP sites in the
434 Hefei region. Figure S5 shows the comparison between the simulated and observed
435 diurnal variations of PM_{2.5} averaged over the study period. The model captures the key
436 features of the observed diurnal cycle well, including the nocturnal accumulation of
437 PM_{2.5} under stable boundary layer conditions and the daytime concentration decrease
438 driven by boundary layer development and enhanced turbulent mixing. The simulated
439 diurnal variation are generally consistent with observations, while the overestimation
440 of nighttime concentrations is primarily attributed to insufficient representation of
441 turbulent mixing intensity under stable nocturnal boundary layer conditions in the
442 model (Yang et al., 2025).

443 It is worth noting that the Nolake experiment, in which Chaohu Lake is replaced
444 by cropland, is a controlled sensitivity experiment designed to isolate lake-induced

445 effects and does not represent an observable atmospheric state, so independent
446 observational validation is neither feasible nor necessary. Given the overall satisfactory
447 performance of the Lake experiment demonstrated above, the simulation framework is
448 considered reliable, and the lake-induced signals identified through the differential
449 analysis between the two experiments are sufficiently credible to support the discussion
450 in the following sections.

451

452 3.1.1 Diurnal reversal of lake effects on near-surface PM_{2.5} concentrations

453 The spatial distribution of PM_{2.5} near-surface concentrations (the lowest model
454 level) in the Lake experiment and the differences between the Lake and Nolake
455 experiments at 08:00, 14:00, 20:00, and 02:00 LT, averaged over 10-20 March 2019, is
456 illustrated in Figure 3. Unless otherwise specified, all analyses presented in this study
457 represent temporal averages over the 10-day period from 10 to 20 March 2019. At 08:00
458 LT (Figure 3a), significant PM_{2.5} pollution centers appeared in urban areas where
459 concentrations typically exceeded 70 $\mu\text{g}/\text{m}^3$, while lake area concentrations in the Lake
460 experiment reached 50-60 $\mu\text{g}/\text{m}^3$. Figure 3b presents that PM_{2.5} concentrations over the
461 lake region in the Lake experiment significantly exceeded those in the Nolake
462 experiment, with the differences predominantly ranging from 0 to 10 $\mu\text{g}/\text{m}^3$ and
463 exceeding 10 $\mu\text{g}/\text{m}^3$ in some regions. Additionally, the lake presence induced varying
464 degrees of PM_{2.5} concentration enhancement in urban areas to the north and northwest.
465 These results indicate that the lake enhances pollutant accumulation over its surface
466 and facilitates transport to surrounding regions through atmospheric dispersion, thereby
467 exacerbating urban PM_{2.5} pollution during morning. At 14:00 LT, PM_{2.5} concentrations
468 throughout the region decreased substantially (Figure 3c), with urban concentrations
469 declining to approximately 30–40 $\mu\text{g}/\text{m}^3$ due to daytime boundary layer development
470 and enhanced dispersion. Over the lake area, PM_{2.5} concentrations in the Lake
471 experiment approached 40 $\mu\text{g}/\text{m}^3$, comparable to urban concentrations and substantially
472 higher than corresponding values in the Nolake experiment. The difference shown in
473 Figure 3d reveals that the lake's pollution-enhancing effect peaked during afternoon.
474 Specifically, PM_{2.5} concentrations in the Lake experiment over the lake surface

475 significantly exceeded those in the Nolake experiment by more than $10 \mu\text{g}/\text{m}^3$.
476 Compared to 8:00 LT, pollutant dispersion from the lake surface to surrounding areas
477 extended over greater distances in the Lake experiment, with more pronounced relative
478 differences in concentrations. Significant concentration enhancement zones of 0–10
479 $\mu\text{g}/\text{m}^3$ form around the lake perimeter. These results indicate that the lake’s pollution-
480 enhancing effect intensifies during the afternoon and further exacerbates air pollution
481 in surrounding urban areas.

482 To further support the reliability of the simulated $\text{PM}_{2.5}$ accumulation over the
483 lake surface, we examine the spatial distribution of satellite-derived hourly high-
484 resolution near-surface $\text{PM}_{2.5}$ data over eastern China from the ChinaHigh $\text{PM}_{2.5}$ dataset
485 (Wei et al., 2021), which provides hourly near-surface $\text{PM}_{2.5}$ concentrations during
486 08:00–17:00 LT. The corresponding results are shown in Figure S6. It should be
487 emphasized that this comparison is not intended as a quantitative validation of our
488 simulation results. The ChinaHigh $\text{PM}_{2.5}$ data used here are from 2018 rather than the
489 simulated period of March 2019, precluding an exact temporal match with our model
490 output. In addition, satellite-derived $\text{PM}_{2.5}$ estimates are subject to inherent retrieval
491 uncertainties, particularly over water surfaces, which renders meaningful quantitative
492 comparison with model output unfeasible. Figure S6 is therefore presented purely for
493 qualitative purposes, to demonstrate that elevated $\text{PM}_{2.5}$ concentrations over the lake
494 surface relative to surrounding areas represent a physically plausible phenomenon
495 supported by independent observational evidence, rather than an artifact of the model
496 configuration. Figure S6 shows that daytime lake-surface $\text{PM}_{2.5}$ is comparable to or
497 exceeds that over adjacent urban areas, with this feature being most pronounced during
498 11:00–16:00 LT (Figures S6d–i), which is qualitatively consistent with the
499 accumulation mechanism identified in our simulations. We acknowledge that direct
500 quantitative validation of lake-surface $\text{PM}_{2.5}$ using in-situ observations would be highly
501 desirable. Unfortunately, in-situ air quality observations over lake surfaces and
502 shoreline areas remain extremely scarce in China, with very limited publicly available
503 data. Targeted observational deployments are discussed further in Sect. 4.

504 During nighttime, the lake impact on surrounding air quality underwent a

505 fundamental reversal. At 20:00 LT, regional $PM_{2.5}$ concentrations increased rapidly due
506 to reduced nighttime PBLH and deteriorated dispersion conditions, as shown in Figure
507 3e. In urban areas, $PM_{2.5}$ concentrations in the Lake experiment exceeded $80 \mu\text{g}/\text{m}^3$,
508 while concentrations over the lake surface ranged from approximately $40\text{--}50 \mu\text{g}/\text{m}^3$.
509 Figure 3f clearly demonstrates that $PM_{2.5}$ concentrations over the lake surface in the
510 Lake experiment remained higher than those in the Nolake experiment, with the
511 differences predominantly ranging from 0 to $10 \mu\text{g}/\text{m}^3$ and exceeding $10 \mu\text{g}/\text{m}^3$ in some
512 regions. However, the lake presence significantly reduced $PM_{2.5}$ concentrations in
513 urban areas to its north and northwest, with reductions generally exceeding $10 \mu\text{g}/\text{m}^3$.
514 This phenomenon indicates that the lake exerted a distinct and continuous purification
515 effect on surrounding urban areas during nighttime. By 2:00 LT, high-concentration
516 pollution masses continued to persist and accumulate in urban areas, with
517 concentrations in the central urban area exceeding $90 \mu\text{g}/\text{m}^3$ (Figure 3g). The lake area
518 maintained higher concentrations in the Lake experiment compared to the Nolake
519 experiment (Figure 3h). The nighttime purification effect persisted at 02:00 LT, with
520 $PM_{2.5}$ concentrations in the Lake experiment remaining lower in urban areas by $0\text{--}10$
521 $\mu\text{g}/\text{m}^3$. Although the spatial extent and pattern of the purification effect evolved slightly
522 compared to 20:00 LT, the improvement effect of the lake on urban air quality remained
523 stable and persistent throughout the night. The spatial distributions of $PM_{2.5}$ near-
524 surface concentrations in the Lake and Nolake experiments at 11:00, 17:00, 23:00, and
525 05:00 LT (Figure S7) displayed patterns consistent with those at 08:00, 14:00, 20:00,
526 and 02:00 LT, further validating the stability and reproducibility of the diurnal variation
527 in the lake's impact on local $PM_{2.5}$ concentrations. The lake exhibits significant diurnal
528 variation in its influence on local $PM_{2.5}$ concentrations, consistently maintaining higher
529 concentrations over the lake surface than in the Nolake experiment. The lake's impact
530 on surrounding urban areas shows distinct diurnal differences, enhancing urban $PM_{2.5}$
531 concentrations by $0\text{--}10 \mu\text{g}/\text{m}^3$ (exceeding $10 \mu\text{g}/\text{m}^3$ in some regions) during daytime
532 with peak effects at 14:00 LT, while reducing concentrations by $0\text{--}10 \mu\text{g}/\text{m}^3$ (exceeding
533 $10 \mu\text{g}/\text{m}^3$ in some regions) during nighttime, revealing a dual role in regulating local
534 air quality.

535 Furthermore, to more clearly quantify the PM_{2.5} concentration differences
536 between the Lake and Nolake experiments and their temporal and spatial variations,
537 Figure 4 presents the diurnal variation of PM_{2.5} concentrations along the key path
538 indicated in Figure 3. Figure 4a compares the average PM_{2.5} concentration differences
539 along this transect during daytime (the average of 08:00, 11:00, 14:00, and 17:00) and
540 nighttime (the average of 20:00, 23:00, 02:00, and 05:00). During daytime, the presence
541 of the lake consistently elevates PM_{2.5} concentrations along the transect, with the most
542 significant impact at point B adjacent to the lakeshore (0 km distance), where the peak
543 difference exceeds 8 µg/m³. This effect gradually weakens with increasing distance and
544 stabilizes at 0-2 µg/m³ beyond approximately 15 kilometers. At night, a significant
545 purification effect is observed. At point B, the concentration difference is slightly
546 positive but rapidly becomes negative approximately 1 kilometers from the lakeshore,
547 reaching maximum purification effectiveness in the urban center 16-17 kilometers from
548 point B, with concentration reductions approaching 8 µg/m³. This indicates that the
549 most significant nighttime purification occurs not immediately adjacent to the lakeshore
550 but rather appears in areas at a certain distance from the lakeshore.

551 Figures 4b shows the evolution of PM_{2.5} concentrations along the path with time
552 and distance for the Lake experiments, exhibiting strong diurnal variation. During
553 nighttime to early morning (approximately 19:00–08:00 LT), PM_{2.5} concentrations
554 exceed 70 µg/m³ due to persistent pollutant accumulation under stable boundary layer
555 conditions. During daytime (approximately 09:00–18:00 LT), concentrations decrease
556 significantly to 30-50 µg/m³ as the boundary layer develops and dispersion conditions
557 improve. Figure 4c displays the diurnal variation of PM_{2.5} concentration differences
558 between the Lake and Nolake experiments with distance, revealing the day-night
559 reversal in the impact of the lake. During daytime, PM_{2.5} concentrations are higher in
560 the Lake experiment, with the greatest enhancement occurring in the near-lake area 0-
561 6 kilometers from point B, where the maximum increase exceeds 8 µg/m³, decreasing
562 with increasing distance. Notably, the influence range is most extensive at 14:00 LT,
563 with concentration increases of 2-4 µg/m³ still present within 15 kilometers from the
564 lakeshore, consistent with the daytime performance shown in Figure 4a. At night, PM_{2.5}

565 concentrations decrease, with more significant reductions at certain distances from the
566 shore. For example, at 20:00 LT in the area approximately 12-18 kilometers from point
567 B, maximum reductions exceed $8 \mu\text{g}/\text{m}^3$. To further investigate the diurnal reversal
568 pattern at different times, Figure S8 shows the distribution of average $\text{PM}_{2.5}$
569 concentration differences along the path at eight key moments. The results are highly
570 consistent with Figure 4, revealing in greater detail the intensity variations, influence
571 ranges, and temporal evolution of the pollution enhancement and purification effects.
572 Overall, the lake exerts a strong diurnal regulatory effect on local $\text{PM}_{2.5}$ concentrations,
573 exacerbating pollution in near-shore areas during daytime while providing a
574 purification effect for surrounding urban areas during nighttime.

575

576 3.1.2 Aerosol-species dependent response of $\text{PM}_{2.5}$ to lake effects

577 Furthermore, $\text{PM}_{2.5}$ is composed of different components, yet the diurnal
578 variation characteristics of these different components and their response mechanisms
579 to lake influence remain unclear. To investigate the different impact of the lake on
580 various $\text{PM}_{2.5}$ components, this study conducted an in-depth analysis of primary and
581 secondary $\text{PM}_{2.5}$, as shown in Figures 5A and 5B. During daytime, the difference in
582 secondary $\text{PM}_{2.5}$ concentrations between the Lake and Nolake experiments is
583 substantially larger than that of primary $\text{PM}_{2.5}$. At 14:00 LT (Figures 5Ac, 5Ad, 5Bc
584 and 5Bd), the increase of secondary $\text{PM}_{2.5}$ concentration over the lake is generally 5-10
585 $\mu\text{g}/\text{m}^3$, which is not only significantly greater than the 0-5 $\mu\text{g}/\text{m}^3$ increase in primary
586 $\text{PM}_{2.5}$, but also extends over a broader range and extent of influence in surrounding
587 areas. This spatial pattern reflects a sequential transport process. Particulate matter is
588 first transported from pollution source regions (such as urban areas) to the lake surface,
589 which has no local emissions. Subsequently, due to the suppressed boundary layer
590 height, weak boundary layer mixing, and low dry deposition rates over the lake,
591 particles accumulate substantially on the lake surface (detailed mechanism explained
592 in Section 3.2.2). Notably, secondary $\text{PM}_{2.5}$ concentrations over the lake are 15-18
593 $\mu\text{g}/\text{m}^3$, while secondary $\text{PM}_{2.5}$ concentrations in urban areas in the Lake experiment are
594 approximately 12-15 $\mu\text{g}/\text{m}^3$, forming an anomalous pollution pattern where lake surface

595 concentrations exceed urban concentrations, which differs dramatically from
596 conventional understanding. Moreover, because the accumulation of secondary PM_{2.5}
597 over the lake during daytime is much greater than that of primary PM_{2.5} (detailed
598 mechanism explained in Section 3.2.4), a greater amount of secondary particles is
599 subsequently transported back to urban and other surrounding areas through lake-
600 breeze circulation and dispersion (detailed mechanism explained in Section 3.2.3),
601 becoming a key factor in exacerbating urban daytime PM_{2.5} pollution.

602 During nighttime, however, the dominant mechanism undergoes a fundamental
603 reversal, with physical transport of primary PM_{2.5} becoming the key factor determining
604 changes in total PM_{2.5} concentrations in urban areas. Primary PM_{2.5} concentrations in
605 urban areas are substantially reduced due to the lake presence, while secondary PM_{2.5}
606 reductions are relatively limited. Therefore, primary PM_{2.5} dominate the spatial
607 distribution of PM_{2.5} concentrations in urban areas during nighttime. At 20:00 LT
608 (Figures 5Af and 5Bf), widespread reductions in primary PM_{2.5} concentrations occur
609 across urban areas, with decreases exceeding 10 µg/m³ that correspond closely to the
610 negative difference zones of total PM_{2.5}. In contrast, secondary PM_{2.5} reductions are
611 much weaker, with scattered affected areas and intensities generally ranging between
612 0-2.5 µg/m³, indicating that the nighttime purification effect is primarily achieved
613 through effective removal of directly emitted pollutants (primary PM_{2.5}). Additionally,
614 Figures S9A and S9B show the primary and secondary PM_{2.5} distribution at several
615 other time points, with the overall pattern consistent with these results. In summary, the
616 impact of lake on PM_{2.5} exhibits significant aerosol-species dependent response and
617 diurnal transition characteristics. The nighttime purification effect is dominated by
618 physical removal of primary PM_{2.5}, while the daytime pollution enhancement effect,
619 particularly the formation of extreme concentrations above the lake, is closely related
620 to the unique chemical-physical interactions involving secondary PM_{2.5}.

621

622 **3.2 Factors controlling the variations of PM_{2.5} concentrations over the lake and** 623 **urban areas**

624 To elucidate the fundamental physical and chemical mechanisms underlying the

625 diurnal reversal effect of lakes on PM_{2.5} concentrations, we conducted an in-depth
626 analysis of the evolution of PM_{2.5} and its associated physical, dynamic, and chemical
627 drivers in this section.

628

629 3.2.1 Spatiotemporal evolution of PM_{2.5} vertical distribution

630 Figure 6 presents the vertical cross-section of PM_{2.5} concentrations and wind
631 vectors along the key path AC (as shown in Fig. 2). At 08:00, the PM_{2.5} high-
632 concentration zone in both experiments was primarily concentrated below 0.3 km in
633 urban areas, exceeding 55 µg/m³, while concentrations over the lake region were
634 relatively low. The lake effect had already begun to manifest. Figure 6c shows near-
635 surface PM_{2.5} concentrations over the lake were significantly higher in the Lake
636 experiment, with peak differences exceeding 5 µg/m³, spreading toward surrounding
637 urban areas and maintaining substantial differences at considerable distances from the
638 lakeshore. Notably, near the top of the boundary layer, PM_{2.5} concentrations in the Lake
639 experiment were actually lower than those in the Nolake experiment. At 14:00,
640 although PM_{2.5} concentrations generally decreased to 20-35 µg/m³ due to boundary
641 layer development, the pollution-enhancing effect of the lake peaked. The high-
642 concentration layer extending upward to approximately 1.5 km altitude with more
643 uniform vertical mixing. Figure 6f shows maximum positive concentration differences
644 of approximately 10 µg/m³ over the lake region, extending upward to nearly 1 km in
645 height. This effect significantly spread both horizontally and vertically toward adjacent
646 urban areas, forming an extensive strong positive difference zone in the lakeside region
647 that stretched from the near-surface up to 1.3 km altitude. Compared to 08:00, the
648 afternoon PM_{2.5} concentration increase was larger with broader impact range, further
649 exacerbating air pollution in surrounding urban areas, consistent with the horizontal
650 distribution patterns described earlier.

651 At 20:00 and 02:00 LT (Figures 6g-l), decreased PBLH causes pollutants to re-
652 accumulate near the urban surface, forming a shallow pollution layer exceeding 55
653 µg/m³. Over the lake area, PM_{2.5} concentrations near the lake surface in the Lake
654 experiment remained higher than in the Nolake experiment, while concentrations above

655 the lake surface were lower. In urban areas, the nighttime differences exhibit
656 distribution characteristics completely opposite to daytime. The vertical cross-sections
657 (Figures 6i, l) reveal a “negative below, positive above” difference pattern. Near-surface
658 PM_{2.5} concentrations are lower in the Lake experiment with maximum decreases of
659 approximately 15 μg/m³, while at higher boundary layer levels, the situation is
660 completely reversed, PM_{2.5} concentrations are higher in the Lake experiment by
661 approximately 0-10 μg/m³. Other periods also exhibit the same vertical distribution, as
662 shown in Figure S10.

663

664 3.2.2 Lake-induced meteorological regulation and the accumulation of PM_{2.5} over the 665 lake

666 The unique physical properties of lakes constitute the intrinsic mechanism
667 underlying these concentration variations. First, the lake significantly suppresses
668 boundary layer development above its surface. As shown in Figure 6, the PBLH over
669 the lake surface in the Lake experiment is markedly lower than in the Nolake
670 experiment, particularly at 14:00 (Figure 6d), where it was suppressed to an extremely
671 shallow level of less than 0.1 km while the boundary layer in the Nolake experiment
672 had developed to nearly 1.5 km. This reduced PBLH inhibits the upward dispersion of
673 PM_{2.5} from the lake region, causing particles to accumulate over the lake surface and
674 thereby increasing PM_{2.5} concentrations. At 20:00 and 02:00 LT (Figures 6g-l), the
675 nighttime boundary layer height in the Lake experiment remained substantially lower
676 than in the Nolake experiment, strongly inhibiting upward PM_{2.5} diffusion above the
677 lake surface.

678 Second, the lake substantially weakens vertical mixing capacity above it. During
679 daytime, land areas exhibit strong mixing with generally high mixing coefficients,
680 particularly in urban areas where values exceed 15 m²/s, as shown in Figure 7a.
681 However, mixing capacity above the lake is significantly suppressed, with extremely
682 low mixing coefficients of approximately 0-0.4 m²/s. Figure 7b demonstrates that the
683 lake presence greatly reduced daytime boundary layer mixing intensity compared to the
684 Nolake experiment. During nighttime, the PBL mixing coefficient above the lake in the

685 Lake experiment remained over 40% lower than in the Nolake experiment (Figure 7d).
686 This weakened mixing stems from two primary mechanisms. First, the large specific
687 heat capacity of lake water causes slow daytime warming, resulting in surface
688 temperatures lower than those of surrounding land. This thermal contrast creates stable
689 atmospheric stratification that suppresses vertical thermal turbulence, leading to rapid
690 $PM_{2.5}$ accumulation over the lake surface. Second, the significantly lower aerodynamic
691 roughness of the lake surface compared to land plays a crucial role. The smooth water
692 surface generates considerably less mechanical turbulence (wind shear) than the
693 rougher farmland surface in the Nolake experiment. Consequently, the lack of
694 mechanical mixing further inhibits vertical diffusion, maintaining the storage effect of
695 the lake.

696 Furthermore, dry deposition velocity differs significantly between the lake and
697 land surface. Figure 8 shows the spatial distribution of dry deposition velocity in the
698 study area. Daytime land areas, especially urban surfaces, exhibit relatively high dry
699 deposition velocity reaching up to 0.045 m/s. However, dry deposition velocity over
700 the lake in the Lake experiment was extremely low, approaching zero, while in the
701 Nolake experiment, the farmland surface replacement increased dry deposition velocity
702 dramatically to 0.025-0.03 m/s (Figure 8a). Figure 8b clearly shows that the lake
703 significantly reduced the dry deposition velocity in this region. During nighttime, the
704 lake also significantly reduced dry deposition velocity above its surface, with decreases
705 far exceeding 10% (Figure 8d). This indicates that the lake water body acts as an
706 extremely inefficient deposition surface, making it difficult for pollutants to settle on
707 its surface, directly leading to prolonged $PM_{2.5}$ lifetimes and more pronounced pollution
708 accumulation in the near-surface boundary layer.

709 Figure 9 further illustrates the spatial distribution of $PM_{2.5}$ lifetimes in the study
710 area. During daytime, land areas show relatively short $PM_{2.5}$ lifetimes, particularly in
711 urban areas where they are only 50-100 hours attributed to higher dry deposition rates
712 that promote pollutant removal. In the Lake experiment (Figure 9a), $PM_{2.5}$ lifetimes
713 over the lake surface exhibited extremely high values exceeding 1500 hours, forming a
714 stark contrast with surrounding land areas. Figure 9b shows that the lake presence even

715 increased PM_{2.5} lifetimes above its surface by over 800 hours. During nighttime, the
716 lake similarly extended pollutant lifetimes (Figure 9d), with maximum increases of
717 approximately 500 hours. This demonstrates that the combined effects of the
718 compressed boundary layer, weak turbulent mixing, and significantly reduced dry
719 deposition velocity over the lake work synergistically to inhibit PM_{2.5} removal in the
720 lake region, making the lake a “storage zone” for particles, thereby causing strong near-
721 surface pollutant accumulation.

722

723 3.2.3 Lake-induced transport regulation and the redistribution of PM_{2.5} in urban areas

724 While physical mechanisms lead to pollutant accumulation, dynamic processes
725 drive the transport and redistribution of these particles. Pollutants are first transported
726 from source regions (such as urban areas) to the lake surface, which has no local
727 emissions. Subsequently, the suppressed boundary layer height, weakened turbulent
728 mixing, and reduced dry deposition velocity over the lake cause PM_{2.5} to accumulate
729 substantially near the surface, resulting in near-surface PM_{2.5} concentrations in the Lake
730 experiment being substantially higher than in the Nolake experiment over the lake area.
731 However, this accumulation is largely confined to the near-surface layer. At upper levels,
732 the pattern reverses. The Nolake experiment shows higher PM_{2.5} concentrations as
733 stronger thermal turbulence from the farmland surface mixes more pollutants to higher
734 altitudes, whereas the Lake experiment maintains a more stable atmosphere that
735 suppresses vertical mixing. This mechanism operates consistently during both daytime
736 and nighttime, as validated by the vertical profiles of PM_{2.5} concentrations in Figure
737 S11. Figures S11b and S11d demonstrate that over the lake area, PM_{2.5} concentrations
738 in the Lake experiment remain higher near the surface but lower aloft than in the Nolake
739 experiment throughout the diurnal cycle. This vertically-stratified pollution structure
740 over the lake represents only the direct local effect. The lake’s influence extends to
741 surrounding urban areas through complex dynamical transport processes that
742 redistribute the accumulated pollutants both horizontally and vertically back to urban
743 and other surrounding areas. These lake-induced perturbations to urban areas exhibit
744 distinct mechanisms during daytime (horizontal convergence and frontal stagnation)

745 and nighttime (enhanced vertical redistribution). These dual mechanisms govern the
746 spatiotemporal patterns of lake-urban PM_{2.5} interactions and explain the observed
747 diurnal reversal effect in urban air quality.

748 During daytime, this influence manifests primarily through horizontal transport
749 processes coupled with lake breeze-background wind interactions. High-pollution air
750 masses formed over the lake affect surrounding urban areas through horizontal transport
751 by concentration gradients between the lake and city. As PM_{2.5} concentrations over the
752 lake increase significantly, pollutants diffuse outward, creating a positive difference
753 layer extending from the lake to the city from the surface to nearly 1 km altitude, with
754 maximum concentration differences of approximately 10 µg/m³. The dramatic PM_{2.5}
755 increases in specific lakefront regions, particularly the southwestern shore, result from
756 intense dynamical interactions between lake breeze circulation and the background
757 wind field. At 14:00 LT, peak solar radiation creates maximum lake-land temperature
758 differences, driving lake breeze formation that radiates outward and superimposes on
759 the prevailing southwest wind (Figure 10d). In the southwestern lake region, the
760 northeastward lake breeze meets the background southwest wind head-on, forming a
761 persistent convergence line termed the “lake breeze front” that acts as a dynamical
762 barrier. This front creates a horizontal stagnation zone with sharply reduced wind
763 speeds (Figure 10f), trapping high-concentration pollutants diffusing from the lake and
764 those carried by the background wind, causing concentrations to spike. Figure S12
765 shows wind speed at other times, displaying varying degrees of daytime dynamical
766 convergence. Cross-sectional analysis along pathway AC (Figure 6d) further confirms
767 this mechanism, showing airflow from the urban area being strongly lifted by lake-area
768 airflow near the lakeshore, blocking background airflow advance and forcing strong
769 upward motion, a typical characteristic of convergence zones absent in the Nolake
770 experiment. At the northern shore, the southward lake breeze converges with the
771 westward background wind, creating less intense but still significant convergence. At
772 the northeastern shore, the lake breeze aligns with the background southwest wind,
773 preventing frontal convergence, so pollutant accumulation results solely from diffusion
774 with much smaller intensity. While lake-induced meteorological perturbations to urban

775 areas remain relatively limited during daytime due to vigorous urban boundary layer
776 development, intense turbulent mixing, and strong dry deposition velocity (Figures 7b
777 and 8b), the lake breeze-driven convergence mechanism creates localized “pollutant
778 stagnation traps” at strategic locations where opposing wind systems meet,
779 fundamentally altering pollution patterns along specific lakefront areas.

780 In stark contrast to the daytime horizontal convergence and gradient-driven
781 diffusion, nighttime dynamics are dominated by enhanced vertical redistribution that
782 reverses the lake’s effect on near-surface urban air quality. As shown in Figures 6i and
783 6l, the urban area exhibits a distinct “negative-below, positive-above” difference pattern
784 stemming from lake-induced perturbation effect. Figure 11 reveals the underlying
785 mechanism by showing the net contribution of vertical mixing to PM_{2.5} concentrations
786 along path AC. In urban areas under both scenarios (Figures 11a, b), vertical mixing
787 presents a “negative below, positive above” contribution pattern. Near the surface,
788 pollutants are transported upward by turbulent mixing, leading to strong negative
789 contributions below -16 μg/m³. Meanwhile, within the boundary layer above
790 (approximately below 0.3 km), strong positive contributions far exceeding +16 μg/m³
791 occur due to pollutants reception from below. The difference between experiments
792 (Figure 11c) reveals that near the urban surface, negative difference values indicate
793 greater concentration reduction in the Lake experiment, while positive values aloft
794 indicate greater concentration increases, demonstrating that PBL vertical mixing
795 intensity in urban areas is much greater in the Lake experiment. The underlying
796 mechanism involves land breeze circulation driven by lake-land thermal contrasts,
797 which induces additional dynamic turbulence and upward motion above the city,
798 disrupting typical nighttime stable conditions. This lake-enhanced vertical mixing more
799 efficiently transports accumulated near-surface pollutants upward, achieving effective
800 purification of near-surface urban air. Figure S11c validates these results, showing
801 lower PM_{2.5} concentrations near the urban surface but higher concentrations at 100-300
802 m altitude in the Lake experiment during nighttime, indicating a dynamic process
803 transporting near-surface pollutants upward driven by lake-induced perturbations to
804 urban meteorological fields and PBL vertical mixing processes. Notably, this nighttime

805 concentration reduction in urban areas is primarily attributable to the vertical mixing of
806 primary PM_{2.5} rather than secondary aerosols. As illustrated in Figure S13, nighttime
807 urban areas continue to experience active secondary aerosol formation through
808 chemical reactions, which increases secondary PM_{2.5} concentrations and counteracts
809 the reduction effect from vertical mixing. Consequently, the net decrease in near-
810 surface urban PM_{2.5} concentrations during nighttime predominantly results from the
811 efficient upward transport of primary particles via lake-enhanced vertical mixing, while
812 the reduction of secondary PM_{2.5} is substantially offset by concurrent chemical
813 production.

814

815 3.2.4 Lake-induced chemical regulation and the formation of secondary PM_{2.5}

816 Beyond the physical and dynamical mechanisms discussed above, lakes
817 profoundly influence PM_{2.5} distributions by regulating atmospheric chemical processes,
818 particularly for secondary aerosols. As revealed in Section 3.1.2, secondary PM_{2.5}
819 concentration differences between the Lake and Nolake experiments over the lake
820 region at 14:00 significantly exceed those of primary PM_{2.5}, with lake surface
821 concentrations reaching or exceeding urban levels. This stems from fundamental
822 differences in formation mechanisms and thermodynamic sensitivity. While primary
823 PM_{2.5} (BC, OC, OIN) originates mainly from direct emissions with minimal chemical
824 transformations, secondary PM_{2.5} formation is highly sensitive to temperature and
825 humidity, which lakes powerfully regulate through their large heat capacity. The
826 ammonium nitrate formation process ($\text{NH}_3 + \text{HNO}_3 \rightleftharpoons \text{NH}_4\text{NO}_3$) exhibits
827 thermodynamic reversibility, which decreased temperature or increased humidity
828 promotes particulate NH₄NO₃ formation, while high-temperature and low-humidity
829 cause decomposition into NH₃ and HNO₃ gases. In contrast, sulfate formation through
830 SO₂ oxidation is almost irreversible and demonstrates greater atmospheric stability.

831 At 08:00, chemical contributions remain consistent between experiments,
832 showing weak net production (6-10 μg/m³) in near-surface urban areas due to precursor
833 enrichment from traffic, industrial, and domestic activities, while lake contributions
834 approach zero (Figure S14a, c). At 14:00, however, dramatically different patterns

835 emerge (Figures S14b and S14d). In the Nolake experiment, elevated temperatures and
836 lower humidity below 0.5 km promote NH_4NO_3 decomposition, producing strong
837 negative $\text{PM}_{2.5}$ contributions (exceeding $-16 \mu\text{g}/\text{m}^3$), while turbulent transport carries
838 decomposed precursors to 0.5-1.5 km altitudes where lower temperatures and higher
839 humidity favor re-condensation, creating strong positive contributions (exceeding 16
840 $\mu\text{g}/\text{m}^3$). Conversely, the Lake experiment shows near-zero chemical contributions
841 throughout the lake area from surface to upper atmosphere. Higher humidity and slower
842 temperature increases due to large heat capacity enhance NH_4NO_3 stability and
843 suppress decomposition, reducing near-surface decomposition, cutting off precursor
844 transport to higher altitudes, and minimizing chemical influence due to weak vertical
845 transport and mixing. These combined effects result maximum nitrate and ammonium
846 concentration differences between experiments at 14:00, with nitrates and ammonium
847 passively accumulating over the lake exceeding urban concentrations (Figures S15 and
848 S16). In comparison, sulfate differences remain much smaller (Figure S17) due to
849 sulfate's irreversible formation and atmospheric stability. In summary, lakes impact
850 secondary $\text{PM}_{2.5}$ during daytime more than primary $\text{PM}_{2.5}$ by regulating local
851 temperature and humidity, profoundly intervening in reversible chemical equilibria and
852 transforming themselves from passive surface types into efficient pollutant "storage
853 zones."

854

855 **3.3 $\text{PM}_{2.5}$ near-surface concentrations over lake and urban areas during daytime** 856 **and nighttime under artificial lake emission scenarios**

857 The preceding analysis systematically revealed the complex lake effect on $\text{PM}_{2.5}$
858 concentrations through meteorological field alterations under the idealized zero-
859 emission lake scenario. However, practical air quality modeling faces pervasive
860 uncertainty from limited emission inventory spatial resolution. Most current inventories
861 cannot effectively distinguish land from lake areas, erroneously assigning emissions to
862 lakes that should have none. This systematic bias may significantly alter lake effects.
863 To assess the real impact of such emission configuration on regional air pollution and
864 lake-urban interactions, we designed two additional control experiments (Lake_emis

865 and Nolake_emis) retaining original emission settings over lake surfaces, with all other
866 parameters consistent with previous two experiments (Lake and Nolake). Comparing
867 these experiments thoroughly investigates how lake surface emissions, prevalent in
868 current simulations, impact PM_{2.5} distribution in surrounding urban areas.

869 Figure 12 shows the spatial distribution of near-surface PM_{2.5} concentrations in
870 the Lake_emis experiment and differences between Lake_emis and Nolake_emis at
871 08:00, 14:00, 20:00, and 02:00 under the scenario retaining the original emission
872 inventory over lake surfaces. At 08:00 (Figures 12a-b), high pollution centers remain
873 in urban areas with concentrations exceeding 80 µg/m³ regardless of lake presence, with
874 peak concentration differences in the lake area exceeding 20 µg/m³. At 14:00 (Figures
875 12c-d), the lake area becomes an extremely prominent pollution hotspot with
876 concentrations reaching 50-80 µg/m³, far exceeding urban concentrations of 35-40
877 µg/m³. Compared to the scenario without lake emissions (Figure 3d), positive
878 differences intensify dramatically in the lake region with peak values approaching 60
879 µg/m³, while surrounding areas also exhibit strong positive differences, indicating that
880 direct daytime lake emissions synergize with physical accumulation mechanisms to
881 jointly exacerbate pollution over the lake and surrounding urban areas. Figures S18a-d
882 confirm this pattern persists at 11:00 and 17:00. At 20:00 (Figures 12e-f), regional
883 pollution rises again with high concentrations centered in urban areas, while the lake
884 region maintains strong positive differences due to continuous emissions combined
885 with weak nighttime boundary layer mixing and low dry deposition. However, urban
886 areas still exhibit significant negative differences with maximum reductions are
887 approximately 30 µg/m³, demonstrating that the lake's physical purification mechanism
888 for urban areas persists even with lake surface emissions. At 02:00 (Figures 12g-h),
889 urban pollution remains elevated while concentration differences stay negative at
890 approximately -20 µg/m³, further confirming the lake's significant nighttime
891 purification effect. Notably, both positive and negative differences coexist in the lake
892 region, potentially reflecting complex physicochemical mechanisms introduced by lake
893 emissions. Figures S18e-h at 23:00 and 05:00 confirm these phenomena.

894 Furthermore, Figure 13 shows the vertical cross-sections of PM_{2.5} concentrations

895 along the AC pathway under the retained lake emission scenario, revealing how lake
896 emissions alter PM_{2.5} vertical structure. During daytime, lake surface emissions
897 synergize with the lake's intrinsic physical properties, emerging at 08:00 and peaking
898 at 14:00. At 08:00 (Figures 13a-c), although high-concentration zones in both
899 experiments remain near the urban surface, differences already reveal significant
900 positive layers over the lake area. By 14:00 (Figures 13d-f), this difference amplifies
901 dramatically. While the Nolake_emis experiment confines high pollution to the deep
902 urban boundary layer, Lake_emis experiment transforms the lake into a new pollution
903 core with intensity far exceeding the city, with PM_{2.5} hotspots exceeding 55 µg/m³
904 hovering over the lake. Differences (Figure 13f) show large positive areas exceeding
905 40 µg/m³ covering the entire lake area and surroundings. Figures S19a-f confirm similar
906 distributions at 11:00 and 17:00, demonstrating that direct lake emissions synergize
907 with unique daytime physical accumulation mechanisms such as compressed boundary
908 layers and weak dry deposition, making the lake an anomalous pollution source
909 exceeding major urban sources. Nighttime cross-sections (Figures 13g-l) confirm that
910 even with lake emissions, the lake-driven physical purification mechanism significantly
911 effects urban areas through persistent negative differences near the surface (Figures 13i,
912 l), while positive and negative differences coexist over the lake, potentially reflecting
913 complex physicochemical mechanisms triggered by lake emissions. Figures S19g-l
914 show similar patterns at 23:00 and 05:00. In summary, these comparative experiments
915 confirm that treatment of lake emissions profoundly affects assessment of lake
916 environmental effects. Retaining lake emissions synergizes with physical accumulation
917 mechanisms to significantly amplify apparent daytime pollution enhancement, while
918 nighttime urban physical purification remains significant. Accurately characterizing
919 underlying surface emissions is crucial for correctly quantifying the dual role lakes play
920 through daytime pollution enhancement and nighttime purification.

921

922 **4. Conclusion and Discussion**

923 Lakes significantly alter local meteorological conditions through thermal

924 contrasts with surrounding surfaces, influencing air pollutant transport and
925 accumulation in adjacent urban areas. While extensive research has examined lake
926 effects on ozone, systematic investigation into lake impacts on PM_{2.5} and its
927 components remains lacking, particularly regarding coupling between lake-induced
928 physical processes (circulation, mixing, deposition) and chemical transformation. This
929 study systematically reveals lake effects on PM_{2.5} and its components within a lake-
930 urban system, elucidating regional PM_{2.5} evolution patterns through physical-chemical
931 coupling mechanisms under lake influence.

932 We investigated the lake effect on PM_{2.5} concentrations during a spring pollution
933 episode (March 2019) through high-resolution WRF-Chem simulations with Lake and
934 Nolake scenarios centered on the Lake Chaohu and Hefei region. During daytime, the
935 lake significantly enhances PM_{2.5} accumulation, with concentrations over the lake
936 surface exceeding those in the Nolake experiment by 0–10 µg/m³ (exceeding 10 µg/m³
937 in some regions) and reaching levels comparable to or higher than urban areas,
938 particularly at 14:00 LT when the pollution-enhancing effect peaks. This daytime
939 enhancement extends to surrounding urban areas, gradually weakening with distance.
940 Satellite observations validate this anomalous daytime accumulation over the lake
941 surface. During nighttime, however, the lake's impact fundamentally reverses, reducing
942 urban PM_{2.5} concentrations by approximately 0-10 µg/m³ (exceeding 10 µg/m³ in some
943 regions), with maximum purification effects occurring 12-18 kilometers from the
944 lakeshore rather than in immediately adjacent areas. Notably, this diurnal reversal
945 exhibits strong component-dependency. Component analysis demonstrates that
946 secondary PM_{2.5} dominates daytime pollution enhancement, with increases of 5-10
947 µg/m³ significantly exceeding primary PM_{2.5} increases of 0-5 µg/m³. The accumulation
948 of secondary particles over the lake, subsequently transported to urban areas by lake
949 breeze and dispersion, is a key mechanism worsening urban daytime pollution.
950 Conversely, nighttime purification is primarily driven by physical removal of primary
951 PM_{2.5}, with reductions exceeding 10 µg/m³ in urban areas, while secondary PM_{2.5}
952 reductions remain limited to 0-2.5 µg/m³. The diurnal reversal of lake effects on PM_{2.5}
953 identified here both corroborates and extends prior findings. Earlier studies on the North

954 American Great Lakes demonstrated that lake-breeze circulations promote recirculation
955 of primary and secondary pollutants and enhance aerosol formation rates (Brook et al.,
956 2013; Hayden et al., 2011), consistent with the daytime urban PM_{2.5} enhancement
957 quantified in the present study. The anomalous daytime PM_{2.5} accumulation over the
958 lake surface is qualitatively analogous to the confinement of urban pollution
959 documented by Dye et al. (1995) over Lake Michigan and the elevated near-surface O₃
960 concentrations reported by Wang et al. (2023) for Lake Taihu. These findings
961 demonstrate that lakes play a complex dual role in regulating regional air quality
962 through distinct physical-chemical mechanisms during day and night.

963 To elucidate the diurnal reversal mechanism, we analyzed the physical,
964 dynamical, and chemical drivers of PM_{2.5} evolution. Lakes suppress boundary layer
965 development, reduce turbulent mixing, and decrease dry deposition velocity, with
966 effects persisting throughout the diurnal cycle but varying in intensity. These combined
967 effects extend lake surface PM_{2.5} lifetimes by over 800 hours during daytime and
968 approximately 500 hours during nighttime, effectively transforming lakes into particle
969 “storage zones.” Lake-land thermal contrasts drive distinct transport regimes during
970 different periods. During daytime, lake breeze-background wind interactions create
971 convergence zones along lakeshores that trap pollutants, increasing concentrations by
972 up to 10 µg/m³ from the surface to nearly 1 km altitude. At night, land breeze circulation
973 enhances urban vertical mixing, purifying near-surface PM_{2.5} by up to 16 µg/m³ while
974 elevating concentrations aloft. This dual mechanism explains the diurnal reversal effect
975 on urban air quality. In addition, lakes regulate local temperature and humidity,
976 suppressing thermal decomposition of ammonium nitrate and other secondary aerosols,
977 with secondary PM_{2.5} differences substantially exceeding those of primary particles.
978 These chemical-physical coupling mechanisms, not previously articulated in lake-
979 urban pollution studies, operate synergistically to shape the complex spatiotemporal
980 patterns of PM_{2.5} interactions between lakes and urban areas.

981 To assess the impact of emission inventory uncertainty on lake-urban PM_{2.5}
982 interactions, we conducted additional experiments (Lake_emis and Nolake_emis)
983 retaining the artificial emission settings over lake surfaces, as most inventories

984 erroneously assign anthropogenic emissions to lakes. Results show that emission
985 treatment profoundly affects lake effect assessments. During daytime, lake emissions
986 synergize with physical accumulation mechanisms to transform the lake area into a
987 prominent pollution hotspot with concentrations reaching 50-80 $\mu\text{g}/\text{m}^3$, exceeding
988 urban levels of 35-40 $\mu\text{g}/\text{m}^3$ at 14:00. Peak concentration differences approach 60 $\mu\text{g}/\text{m}^3$,
989 significantly amplifying the apparent pollution enhancement compared to the zero-
990 emission scenario. During nighttime, the lake-driven purification mechanism persists,
991 with near-surface urban concentration reductions reaching approximately 30 $\mu\text{g}/\text{m}^3$ at
992 20:00 and 20 $\mu\text{g}/\text{m}^3$ at 02:00. These findings confirm that accurate emission
993 characterization is crucial for quantifying lakes' complex role in regional air quality,
994 and further suggest that previous high-resolution air quality modeling studies over lake-
995 containing domains may have erroneously attributed emission-driven pollution
996 hotspots to lake meteorological effects, thereby systematically overestimating the
997 contribution of the lake itself to the spatial distribution of $\text{PM}_{2.5}$. However, most current
998 emission inventories lack sufficient spatial resolution to distinguish water surfaces from
999 land, often erroneously assigning anthropogenic emissions to lake areas and biasing
1000 lake effect assessments. Although Zhang et al. (2017) conducted a similar lake-
1001 replacement sensitivity experiment for ozone over Lake Taihu, their study did not
1002 address the treatment of emissions over water surfaces, an oversight that appears to be
1003 prevalent across similar studies. Therefore, the explicit zeroing of anthropogenic
1004 emissions over water surfaces during the preprocessing stage of regional air quality
1005 simulations should be established as a standardized procedure, a requirement that
1006 becomes increasingly urgent as China's emission inventories are continuously refined
1007 under the impetus of clean air action policies (Geng et al., 2024a; Geng et al., 2024b).
1008 Developing emission inventories that accurately characterize surface-specific emission
1009 patterns is crucial for reliable assessment of lake-urban air quality interactions and
1010 effective pollution control strategies.

1011 While this study provides valuable insights into lake effects on $\text{PM}_{2.5}$
1012 distributions, several considerations emerge regarding broader applicability and future
1013 research directions. It is important to emphasize that while this study centers on the

1014 Lake Chaohu and Hefei system, the identified mechanisms governing the diurnal
1015 evolution of $PM_{2.5}$ are rooted in fundamental physical principles rather than site-
1016 specific coincidences. The intrinsic properties of a lake surface, notably its high thermal
1017 capacity and low aerodynamic roughness, are universal physical attributes that
1018 consistently distinguish water bodies from terrestrial surfaces regardless of geographic
1019 location. These characteristics drive the suppression of PBL development and
1020 mechanical turbulence while leading to characteristically low dry deposition velocities.
1021 Such processes collectively facilitate the formation of atmospheric storage zones that
1022 prolong pollutant lifetimes and create potential pollution reservoirs over the water. At
1023 night, the presence of the lake enhances turbulent mixing in the urban area, thereby
1024 promoting the purification of near-surface pollutants in the adjacent city. Combined
1025 with thermodynamic regulation of secondary aerosol formation, these surface contrasts
1026 establish lakes as dual regulators that both enhance and purify pollution. This may
1027 represent a widespread atmospheric phenomenon characteristic of urban-lake
1028 interfaces globally rather than an isolated case. However, we acknowledge that the
1029 specific manifestation and magnitude of these lake effects are modulated by local
1030 environmental factors, such as topography, emission intensity, and background wind
1031 fields. These conditions determine the precise horizontal and vertical redistribution of
1032 pollutants and the exact location of convergence zones. Therefore, while our findings
1033 provide a generalized framework for understanding lake-atmosphere-pollution
1034 coupling, the exact impact in other regions remains dependent on the local
1035 environmental configuration. By elucidating these universal physical drivers, this study
1036 provides a transferable scientific basis for air quality assessment and forecasting in
1037 lake-adjacent regions worldwide.

1038 The lake effects revealed in this study should be interpreted in the context of the
1039 meteorological background and the limitations of the simulation period. This study
1040 aims to quantitatively isolate the net lake impacts on $PM_{2.5}$ and identify the underlying
1041 physical-chemical mechanisms through high-resolution sensitivity experiments, rather
1042 than conducting long-term climatological statistical analysis, given the extremely high
1043 computational cost of 1-km resolution WRF-Chem simulations. The selected period in

1044 March 2019 corresponds to the pollution season when $PM_{2.5}$ concentrations are
1045 typically much higher than in summer, and lake-land thermal contrasts remain
1046 sufficiently strong to drive significant lake-breeze circulations. However, this study is
1047 not statistically representative of all pollution seasons. The 850 hPa wind fields from
1048 ERA5 reanalysis for January, March, and October (Figure S1) indicate significant
1049 differences in large-scale circulation patterns over eastern China across winter, spring,
1050 and autumn. January is more strongly controlled by winter monsoon circulation, March
1051 exhibits a transitional circulation pattern, while October shows distinct autumn
1052 circulation characteristics different from the former two. This implies that the intensity,
1053 spatial extent, and even the dominant pathways of lake impacts on $PM_{2.5}$ may vary with
1054 seasonal circulation backgrounds. Additionally, the study period was characterized by
1055 predominantly clear skies and moderate background winds, with weak cloud content
1056 and precipitation, which was a deliberate aspect of the study selection strategy to
1057 facilitate the isolation of intrinsic lake effects. Although frontal passages can influence
1058 $PM_{2.5}$ through wind field reorganization, boundary layer structural adjustments, thermal
1059 changes, and wet scavenging processes, this study was not dominated by persistent,
1060 large-scale, strong frontal precipitation events, and thus frontal scavenging was not a
1061 primary controlling factor in this analysis. Since the Lake and Nolake experiments
1062 employ identical initial and boundary conditions, the synoptic-scale circulation
1063 constitutes a common background forcing in both simulations, and thus the simulation
1064 differences primarily reflect perturbations induced by lake presence. In summary, this
1065 study are more applicable to stable weather conditions similar to this springtime
1066 transitional period. Future research should systematically evaluate lake impacts on
1067 pollutants across multiple seasons and different weather patterns (including frontal
1068 events) to establish a more comprehensive understanding of lake-air quality interactions
1069 and quantify their seasonal and circulation dependencies.

1070 Furthermore, our investigation concentrated on $PM_{2.5}$ and its components, yet
1071 atmospheric pollution involves complex multi-species interactions. The transport
1072 patterns of gaseous pollutants such as SO_2 and NO_2 within lake-land thermal circulation
1073 systems, and their conversion to secondary particulate matter under lake modulation,

1074 deserve comprehensive investigation. Extending analysis to other lake-urban systems
1075 and conducting simultaneous multi-pollutant observations would enhance
1076 understanding of lakes' integrated impacts on regional atmospheric chemistry,
1077 providing scientific foundations for air quality management and multi-pollutant
1078 synergistic control strategies in lake-adjacent regions globally. Technical limitations
1079 also present opportunities for improvement. Although this study employed high-
1080 resolution 1 km simulations, the fine-scale structures of lake-land boundary layers and
1081 mesoscale phenomena such as lake-breeze fronts require even higher spatial resolution
1082 for accurate representation. Current planetary boundary layer parameterization schemes
1083 may contain uncertainties when handling complex surface conditions, particularly in
1084 water-land transition zones. Future research should integrate more sophisticated
1085 numerical methods, develop specialized parameterization schemes for lake-land
1086 interface processes, and optimize dry deposition parameterizations across different
1087 surface types based on expanded observational datasets to enhance model capabilities
1088 in simulating lake micrometeorology and boundary layer dynamics.

1089 Additionally, the key limitation of current lake-urban air quality research is the
1090 scarcity of direct observations over lake surfaces and lakeside regions. Although this
1091 study has validated the simulations against urban observation networks, the most
1092 significant lake effects we identified occur precisely over lake surfaces and nearshore
1093 areas where observational infrastructure is absent. While satellite-retrieved PM_{2.5}
1094 products provide qualitative support for lake surface accumulation phenomena, their
1095 spatiotemporal resolution and retrieval uncertainties over water surfaces are insufficient
1096 to meet the needs for detailed mechanistic validation, underscoring the necessity of
1097 systematic field observations. This observational challenge is particularly acute in
1098 China. Many major cities have developed along inland lakes, yet systematic lake-
1099 atmosphere monitoring remains extremely limited compared to North America and
1100 Europe. Future research should prioritize the establishment of comprehensive
1101 observation networks specifically designed for lake-urban pollution gradients. Such
1102 networks should include monitoring stations deployed at multiple locations along
1103 lakeshores and cross-sectional observations along lake-urban corridors (such as the A-

1104 B-C transect examined in this study) to measure PM_{2.5} concentrations, chemical
1105 composition, and meteorological parameters. Lake-based platform observations (buoys
1106 or low-altitude drones) can capture spatial heterogeneity and transient features such as
1107 lake-breeze fronts, while vertical profiling measurements (tethered balloons, drones, or
1108 ground-based remote sensing) can observe boundary layer structure and lake-land
1109 breeze circulation. Additionally, measurements of dry deposition velocities and surface
1110 fluxes over both lake and land surfaces, combined with dense low-cost sensor networks
1111 monitoring fine-scale spatial patterns, will provide multidimensional data support for
1112 understanding lake effects. These observations will not only directly validate the lake-
1113 induced PM_{2.5} gradients and vertical mixing signals identified in this study but also
1114 reveal small-scale turbulent mixing and chemical transformation mechanisms. Filling
1115 the observational gap in lake environments represents a critical frontier for advancing
1116 air quality research in rapidly urbanizing inland lake regions globally.

1117

1118

1119

1120

1121

1122

1123

1124

1125

1126

1127

1128

1129

1130

1131

1132

1133

1134 **Code and data availability.** The updated USTC version of WRF-Chem can be
1135 downloaded from <https://doi.org/10.5281/zenodo.15702248> or can be obtained from
1136 the corresponding author upon request. The Multi-resolution Emission Inventory for
1137 China (MEIC) at 0.25° x 0.25° resolution for 2019 is available at
1138 <http://meicmodel.org.cn> (last access: 11 August 2025) (Li et al., 2017a; Li et al., 2017b;
1139 Zheng et al., 2018; Geng et al., 2024a). The NCEP final reanalysis (FNL) data with a
1140 1° x 1° resolution and 6 h temporal resolution are available at
1141 <https://doi.org/10.5065/D6M043C6> (last access: 11 August 2025) (NCEP, 2000).

1142

1143 **Author contributions.** ZY, QY, and CZ designed the experiments and conducted
1144 and analyzed the simulations. All authors contributed to the discussion and final version
1145 of the paper.

1146

1147 **Competing interests.** The contact author has declared that none of the authors
1148 has any competing interests.

1149

1150 **Disclaimer.** Publisher’s note: Copernicus Publications remains neutral with
1151 regard to jurisdictional claims made in the text, published maps, institutional affiliations,
1152 or any other geographical representation in this paper. While Copernicus Publications
1153 makes every effort to include appropriate place names, the final responsibility lies with
1154 the authors.

1155

1156 **Acknowledgements.** This research was supported by the National Key Scientific
1157 and Technological Infrastructure project “Earth System Numerical Simulation Facility”
1158 (EarthLab). The study used computing resources from the Supercomputing Center of
1159 the University of Science and Technology of China (USTC) and the Qingdao
1160 Supercomputing and Big Data Center.

1161

1162 **Financial support.** This research was supported by the National Key Research
1163 and Development Program of China (grant no. 2023YFC3706300), the Strategic

1164 Priority Research Program of the Chinese Academy of Sciences (grant no.
1165 XDB0500303), the National Natural Science Foundation of China (grant no. 41775146),
1166 the USTC Research Funds of the Double First-Class Initiative (grant nos.
1167 YD2080002007 and KY2080000114), the Science and Technology Innovation Project
1168 of Laoshan Laboratory (grant no. LSKJ202300305), the National Natural Science
1169 Foundation of China (NSFC) Young Students' Basic Research Project (Doctoral
1170 Candidates, grant no. 424B2042), the Innovation Group Project of Southern Marine
1171 Science and Engineering Guangdong Laboratory (Zhuhai) (grant no. 311024009), and
1172 the Southern Marine Science and Engineering Guangdong Laboratory (Zhuhai) (grant
1173 no. SML2024SP011).

1174

1175

1176

1177

1178

1179

1180

1181

1182

1183

1184

1185

1186

1187

1188

1189

1190

1191

1192

1193 **Reference**

1194 Atkinson, B. W.: Meso-scale atmospheric circulations, Academic Press, London, 495
1195 pp.,1981.

1196 Binkowski, F. S. and Shankar, U.: The Regional Particulate Matter Model .1. Model
1197 description and preliminary results, Journal of Geophysical Research-
1198 Atmospheres, 100, 26191-26209, <https://doi.org/10.1029/95jd02093>, 1995.

1199 Brook, J. R., Makar, P. A., Sills, D. M. L., Hayden, K. L., and McLaren, R.: Exploring
1200 the nature of air quality over southwestern Ontario: main findings from the Border
1201 Air Quality and Meteorology Study, Atmospheric Chemistry and Physics, 13,
1202 10461-10482, <https://doi.org/10.5194/acp-13-10461-2013>, 2013.

1203 Burley, J. D., Theiss, S., Bytnerowicz, A., Gertler, A., Schilling, S., and Zielinska, B.:
1204 Surface ozone in the Lake Tahoe Basin, Atmospheric Environment, 109, 351-369,
1205 <https://doi.org/10.1016/j.atmosenv.2015.02.001>, 2015.

1206 Capps, S. L., Hu, Y., and Russell, A. G.: Assessing Near-Field and Downwind Impacts
1207 of Reactivity-Based Substitutions, Journal of the Air & Waste Management
1208 Association, 60, 316-327, <https://doi.org/10.3155/1047-3289.60.3.316>, 2010.

1209 Chai, F., Gao, J., Chen, Z., Wang, S., Zhang, Y., Zhang, J., Zhang, H., Yun, Y., and Ren,
1210 C.: Spatial and temporal variation of particulate matter and gaseous pollutants in
1211 26 cities in China, Journal of Environmental Sciences, 26, 75-82,
1212 [https://doi.org/10.1016/s1001-0742\(13\)60383-6](https://doi.org/10.1016/s1001-0742(13)60383-6), 2014.

1213 Chapman, E. G., Gustafson, W. I., Jr., Easter, R. C., Barnard, J. C., Ghan, S. J., Pekour,
1214 M. S., and Fast, J. D.: Coupling aerosol-cloud-radiative processes in the WRF-
1215 Chem model: Investigating the radiative impact of elevated point sources,
1216 Atmospheric Chemistry and Physics, 9, 945-964, [https://doi.org/10.5194/acp-9-
1217 945-2009](https://doi.org/10.5194/acp-9-945-2009), 2009.

1218 Chen, F. and Dudhia, J.: Coupling an Advanced Land Surface–Hydrology Model with
1219 the Penn State–NCAR MM5 Modeling System. Part I: Model Implementation and
1220 Sensitivity, Monthly Weather Review, 129, 569-585, 2001.

1221 Chen, J. and Hoek, G.: Long-term exposure to PM and all-cause and cause-specific

1222 mortality: A systematic review and meta-analysis, *Environment International*, 143,
1223 <https://doi.org/10.1016/j.envint.2020.105974>, 2020.

1224 Chen, X., Chen, Y., Shimizu, T., Niu, J., Nakagami, K. i., Qian, X., Jia, B., Nakajima,
1225 J., Han, J., and Li, J.: Water resources management in the urban agglomeration of
1226 the Lake Biwa region, Japan: An ecosystem services-based sustainability
1227 assessment, *Science of the Total Environment*, 586, 174-187,
1228 <https://doi.org/10.1016/j.scitotenv.2017.01.197>, 2017.

1229 CMA, 2018: Technical Specifications for Maintenance of Regional Automatic Weather
1230 Stations. QX/T 465–2018. (in Chinese). Available at:
1231 <http://cmastd.cmatc.cn/standardView.jsp?id=3076>. Accessed on 5 May 2022.,
1232 2018.

1233 Dentener, F., Kinne, S., Bond, T., Boucher, O., Cofala, J., Generoso, S., Ginoux, P.,
1234 Gong, S., Hoelzemann, J. J., Ito, A., Marelli, L., Penner, J. E., Putaud, J. P., Textor,
1235 C., Schulz, M., van der Werf, G. R., and Wilson, J.: Emissions of primary aerosol
1236 and precursor gases in the years 2000 and 1750 prescribed data-sets for AeroCom,
1237 *Atmospheric Chemistry and Physics*, 6, 4321-4344, [https://doi.org/10.5194/acp-6-](https://doi.org/10.5194/acp-6-4321-2006)
1238 [4321-2006](https://doi.org/10.5194/acp-6-4321-2006), 2006.

1239 Du, Q., Zhao, C., Zhang, M., Dong, X., Chen, Y., Liu, Z., Hu, Z., Zhang, Q., Li, Y.,
1240 Yuan, R., and Miao, S.: Modeling diurnal variation of surface PM_{2.5} concentrations
1241 over East China with WRF-Chem: impacts from boundary-layer mixing and
1242 anthropogenic emission, *Atmospheric Chemistry and Physics*, 20, 2839-2863,
1243 <https://doi.org/10.5194/acp-20-2839-2020>, 2020.

1244 Dye, T. S., Roberts, P. T., and Korc, M. E.: OBSERVATIONS OF TRANSPORT
1245 PROCESSES FOR OZONE AND OZONE PRECURSORS DURING THE 1991
1246 LAKE-MICHIGAN OZONE STUDY, *Journal of Applied Meteorology*, 34, 1877-
1247 1889, [https://doi.org/10.1175/1520-0450\(1995\)034<1877:Ootpfo>2.0.Co;2](https://doi.org/10.1175/1520-0450(1995)034<1877:Ootpfo>2.0.Co;2), 1995.

1248 Estevez, J., Gavilan, P., and Giraldez, J. V.: Guidelines on validation procedures for
1249 meteorological data from automatic weather stations, *Journal of Hydrology*, 402,
1250 144-154, <https://doi.org/10.1016/j.jhydrol.2011.02.031>, 2011.

1251 Fast, J. D. and Heilman, W. E.: Simulated sensitivity of seasonal ozone exposure in the

1252 Great Lakes region to changes in anthropogenic emissions in the presence of
1253 interannual variability, *Atmospheric Environment*, 39, 5291-5306,
1254 <https://doi.org/10.1016/j.atmosenv.2005.05.032>, 2005.

1255 Fosco, T. and Schmeling, M.: Aerosol ion concentration dependence on atmospheric
1256 conditions in Chicago, *Atmospheric Environment*, 40, 6638-6649,
1257 <https://doi.org/10.1016/j.atmosenv.2006.05.061>, 2006.

1258 Garratt, J. R.: THE INTERNAL BOUNDARY-LAYER - A REVIEW, *Boundary-Layer*
1259 *Meteorology*, 50, 171-203, <https://doi.org/10.1007/bf00120524>, 1990.

1260 Geng, G., Liu, Y., Liu, Y., Liu, S., Cheng, J., Yan, L., Wu, N., Hu, H., Tong, D., Zheng,
1261 B., Yin, Z., He, K., and Zhang, Q.: Efficacy of China's clean air actions to tackle
1262 PM_{2.5} pollution between 2013 and 2020, *Nature Geoscience*, 17,
1263 <https://doi.org/10.1038/s41561-024-01540-z>, 2024a.

1264 Geng, G. N., Liu, Y. X., Liu, Y., Liu, S. G., Cheng, J., Yan, L., Wu, N. N., Hu, H. W.,
1265 Tong, D., Zheng, B., Yin, Z. C., He, K. B., and Zhang, Q.: Efficacy of China's clean
1266 air actions to tackle PM_{2.5} pollution between 2013 and 2020, *Nature Geoscience*,
1267 17, <https://doi.org/10.1038/s41561-024-01540-z>, 2024b.

1268 Guo, H., Cheng, T., Gu, X., Wang, Y., Chen, H., Bao, F., Shi, S., Xu, B., Wang, W., Zuo,
1269 X., Zhang, X., and Meng, C.: Assessment of PM_{2.5} concentrations and exposure
1270 throughout China using ground observations, *Science of the Total Environment*,
1271 601, 1024-1030, <https://doi.org/10.1016/j.scitotenv.2017.05.263>, 2017.

1272 Guo, J., Deng, M., Lee, S. S., Wang, F., Li, Z., Zhai, P., Liu, H., Lv, W., Yao, W., and
1273 Li, X.: Delaying precipitation and lightning by air pollution over the Pearl River
1274 Delta. Part I: Observational analyses, *Journal of Geophysical Research-*
1275 *Atmospheres*, 121, 6472-6488, <https://doi.org/10.1002/2015jd023257>, 2016.

1276 Guo, S., Hu, M., Zamora, M. L., Peng, J., Shang, D., Zheng, J., Du, Z., Wu, Z., Shao,
1277 M., Zeng, L., Molina, M. J., and Zhang, R.: Elucidating severe urban haze
1278 formation in China, *Proceedings of the National Academy of Sciences of the*
1279 *United States of America*, 111, 17373-17378,
1280 <https://doi.org/10.1073/pnas.1419604111>, 2014.

1281 Gustafson, W. I., Jr., Chapman, E. G., Ghan, S. J., Easter, R. C., and Fast, J. D.: Impact

1282 on modeled cloud characteristics due to simplified treatment of uniform cloud
1283 condensation nuclei during NEAQS 2004, *Geophysical Research Letters*, 34,
1284 <https://doi.org/10.1029/2007gl030021>, 2007.

1285 Harris, L. and Kotamarthi, V. R.: The characteristics of the Chicago Lake breeze and
1286 its effects on trace particle transport: Results from an episodic event simulation,
1287 *Journal of Applied Meteorology*, 44, 1637-1654,
1288 <https://doi.org/10.1175/jam2301.1>, 2005.

1289 Hayden, K. L., Sills, D. M. L., Brook, J. R., Li, S. M., Makar, P. A., Markovic, M. Z.,
1290 Liu, P., Anlauf, K. G., O'Brien, J. M., Li, Q., and McLaren, R.: Aircraft study of
1291 the impact of lake-breeze circulations on trace gases and particles during BAQS-
1292 Met 2007, *Atmospheric Chemistry and Physics*, 11, 10173-10192,
1293 <https://doi.org/10.5194/acp-11-10173-2011>, 2011.

1294 He, J., Gong, S., Yu, Y., Yu, L., Wu, L., Mao, H., Song, C., Zhao, S., Liu, H., Li, X.,
1295 and Li, R.: Air pollution characteristics and their relation to meteorological
1296 conditions during 2014-2015 in major Chinese cities, *Environmental Pollution*,
1297 223, 484-496, <https://doi.org/10.1016/j.envpol.2017.01.050>, 2017.

1298 Ho, H. C., Wong, M. S., Yang, L., Shi, W., Yang, J., Bilal, M., and Chan, T.-C.:
1299 Spatiotemporal influence of temperature, air quality, and urban environment on
1300 cause-specific mortality during hazy days, *Environment International*, 112, 10-22,
1301 <https://doi.org/10.1016/j.envint.2017.12.001>, 2018.

1302 Hong, S.-Y., Noh, Y., and Dudhia, J.: A new vertical diffusion package with an explicit
1303 treatment of entrainment processes, *Monthly Weather Review*, 134, 2318-2341,
1304 <https://doi.org/10.1175/mwr3199.1>, 2006.

1305 Hu, J., Wang, Y., Ying, Q., and Zhang, H.: Spatial and temporal variability of
1306 PM_{2.5} and PM₁₀ over the North China Plain and the
1307 Yangtze River Delta, China, *Atmospheric Environment*, 95, 598-609,
1308 <https://doi.org/10.1016/j.atmosenv.2014.07.019>, 2014a.

1309 Hu, J., Zhang, H., Chen, S., Ying, Q., Wiedinmyer, C., Vandenberghe, F., and Kleeman,
1310 M. J.: Identifying PM_{2.5} and PM_{0.1} Sources for Epidemiological Studies in
1311 California, *Environmental Science & Technology*, 48, 4980-4990,

1312 <https://doi.org/10.1021/es404810z>, 2014b.

1313 Hu, L. and Li, Q.: Greenspace, bluespace, and their interactive influence on urban
1314 thermal environments, *Environmental Research Letters*, 15,
1315 <https://doi.org/10.1088/1748-9326/ab6c30>, 2020.

1316 Hu, X.-M. and Xue, M.: Influence of Synoptic Sea-Breeze Fronts on the Urban Heat
1317 Island Intensity in Dallas-Fort Worth, Texas, *Monthly Weather Review*, 144, 1487-
1318 1507, <https://doi.org/10.1175/mwr-d-15-0201.1>, 2016.

1319 Hu, X.-M., Ma, Z., Lin, W., Zhang, H., Hu, J., Wang, Y., Xu, X., Fuentes, J. D., and
1320 Xue, M.: Impact of the Loess Plateau on the atmospheric boundary layer structure
1321 and air quality in the North China Plain: A case study, *Science of the Total
1322 Environment*, 499, 228-237, <https://doi.org/10.1016/j.scitotenv.2014.08.053>,
1323 2014c.

1324 Hu, Z., Huang, J., Zhao, C., Bi, J., Jin, Q., Qian, Y., Leung, L. R., Feng, T., Chen, S.,
1325 and Ma, J.: Modeling the contributions of Northern Hemisphere dust sources to
1326 dust outflow from East Asia, *Atmospheric Environment*, 202, 234-243,
1327 <https://doi.org/10.1016/j.atmosenv.2019.01.022>, 2019.

1328 Huang, R.-J., Zhang, Y., Bozzetti, C., Ho, K.-F., Cao, J.-J., Han, Y., Daellenbach, K. R.,
1329 Slowik, J. G., Platt, S. M., Canonaco, F., Zotter, P., Wolf, R., Pieber, S. M., Bruns,
1330 E. A., Crippa, M., Ciarelli, G., Piazzalunga, A., Schwikowski, M., Abbaszade, G.,
1331 Schnelle-Kreis, J., Zimmermann, R., An, Z., Szidat, S., Baltensperger, U., El
1332 Haddad, I., and Prevot, A. S. H.: High secondary aerosol contribution to particulate
1333 pollution during haze events in China, *Nature*, 514, 218-222,
1334 <https://doi.org/10.1038/nature13774>, 2014.

1335 Iacono, M. J., Mlawer, E. J., Clough, S. A., and Morcrette, J. J.: Impact of an improved
1336 longwave radiation model, RRTM, on the energy budget and thermodynamic
1337 properties of the NCAR community climate model, CCM3, *Journal of Geophysical
1338 Research-Atmospheres*, 105, 14873-14890, <https://doi.org/10.1029/2000jd900091>,
1339 2000.

1340 Janssens-Maenhout, G., Crippa, M., Guizzardi, D., Dentener, F., Muntean, M., Pouliot,
1341 G., Keating, T., Zhang, Q., Kurokawa, J., Wankmueller, R., van der Gon, H. D.,

1342 Kuenen, J. J. P., Klimont, Z., Frost, G., Darras, S., Koffi, B., and Li, M.:
1343 HTAP_v2.2: a mosaic of regional and global emission grid maps for 2008 and 2010
1344 to study hemispheric transport of air pollution, *Atmospheric Chemistry and*
1345 *Physics*, 15, 11411-11432, <https://doi.org/10.5194/acp-15-11411-2015>, 2015.

1346 Jiang, Z., Huo, F., Ma, H., Song, J., and Dai, A.: Impact of Chinese Urbanization and
1347 Aerosol Emissions on the East Asian Summer Monsoon, *Journal of Climate*, 30,
1348 1019-1039, <https://doi.org/10.1175/jcli-d-15-0593.1>, 2017.

1349 Kain, J. S.: The Kain-Fritsch convective parameterization: An update, *Journal of*
1350 *Applied Meteorology*, 43, 170-181, [https://doi.org/10.1175/1520-0450\(2004\)043<0170:Tkcpcpau>2.0.Co;2](https://doi.org/10.1175/1520-0450(2004)043<0170:Tkcpcpau>2.0.Co;2), 2004.

1352 Lei, Y., Zhang, Q., He, K. B., and Streets, D. G.: Primary anthropogenic aerosol
1353 emission trends for China, 1990-2005, *Atmospheric Chemistry and Physics*, 11,
1354 931-954, <https://doi.org/10.5194/acp-11-931-2011>, 2011.

1355 Levy, I., Dayan, U., and Mahrer, Y.: A five-year study of coastal recirculation and its
1356 effect on air pollutants over the East Mediterranean region, *Journal of Geophysical*
1357 *Research-Atmospheres*, 113, <https://doi.org/10.1029/2007jd009529>, 2008.

1358 Levy, I., Makar, P. A., Sills, D., Zhang, J., Hayden, K. L., Mihele, C., Narayan, J.,
1359 Moran, M. D., Sjostedt, S., and Brook, J.: Unraveling the complex local-scale
1360 flows influencing ozone patterns in the southern Great Lakes of North America,
1361 *Atmospheric Chemistry and Physics*, 10, 10895-10915,
1362 <https://doi.org/10.5194/acp-10-10895-2010>, 2010.

1363 Li, H., Ren, G., and Li, W.: Diurnal and intra-season variation of warm-season
1364 temperature in coastal zone of Qinghai Lake, *Theoretical and Applied Climatology*,
1365 138, 1203-1217, <https://doi.org/10.1007/s00704-019-02893-x>, 2019.

1366 Li, M., Liu, H., Geng, G., Hong, C., Liu, F., Song, Y., Tong, D., Zheng, B., Cui, H.,
1367 Man, H., Zhang, Q., and He, K.: Anthropogenic emission inventories in China: a
1368 review, *National Science Review*, 4, 834-866, <https://doi.org/10.1093/nsr/nwx150>,
1369 2017a.

1370 Li, M., Zhang, Q., Kurokawa, J.-i., Woo, J.-H., He, K., Lu, Z., Ohara, T., Song, Y.,
1371 Streets, D. G., Carmichael, G. R., Cheng, Y., Hong, C., Huo, H., Jiang, X., Kang,

1372 S., Liu, F., Su, H., and Zheng, B.: MIX: a mosaic Asian anthropogenic emission
1373 inventory under the international collaboration framework of the MICS-Asia and
1374 HTAP, *Atmospheric Chemistry and Physics*, 17, 935-963,
1375 <https://doi.org/10.5194/acp-17-935-2017>, 2017b.

1376 Li, Y., An, J., and Gultepe, I.: Effects of Additional HONO Sources on Visibility over
1377 the North China Plain, *Advances in Atmospheric Sciences*, 31, 1221-1232,
1378 <https://doi.org/10.1007/s00376-014-4019-1>, 2014.

1379 Li, Z., Guo, J., Ding, A., Liao, H., Liu, J., Sun, Y., Wang, T., Xue, H., Zhang, H., and
1380 Zhu, B.: Aerosol and boundary-layer interactions and impact on air quality,
1381 *National Science Review*, 4, 810-833, <https://doi.org/10.1093/nsr/nwx117>, 2017c.

1382 Li, Z., Li, C., Chen, H., Tsay, S. C., Holben, B., Huang, J., Li, B., Maring, H., Qian, Y.,
1383 Shi, G., Xia, X., Yin, Y., Zheng, Y., and Zhuang, G.: East Asian Studies of
1384 Tropospheric Aerosols and their Impact on Regional Climate (EAST-AIRC): An
1385 overview, *Journal of Geophysical Research-Atmospheres*, 116,
1386 <https://doi.org/10.1029/2010jd015257>, 2011.

1387 Li, Z., Lau, W. K. M., Ramanathan, V., Wu, G., Ding, Y., Manoj, M. G., Liu, J., Qian,
1388 Y., Li, J., Zhou, T., Fan, J., Rosenfeld, D., Ming, Y., Wang, Y., Huang, J., Wang, B.,
1389 Xu, X., Lee, S. S., Cribb, M., Zhang, F., Yang, X., Zhao, C., Takemura, T., Wang,
1390 K., Xia, X., Yin, Y., Zhang, H., Guo, J., Zhai, P. M., Sugimoto, N., Babu, S. S., and
1391 Brasseur, G. P.: Aerosol and monsoon climate interactions over Asia, *Reviews of*
1392 *Geophysics*, 54, 866-929, <https://doi.org/10.1002/2015rg000500>, 2016.

1393 Liu, Z., Gao, W., Yu, Y., Hu, B., Xin, J., Sun, Y., Wang, L., Wang, G., Bi, X., Zhang,
1394 G., Xu, H., Cong, Z., He, J., Xu, J., and Wang, Y.: Characteristics of PM_{2.5} mass
1395 concentrations and chemical species in urban and background areas of China:
1396 emerging results from the CARE-China network, *Atmospheric Chemistry and*
1397 *Physics*, 18, 8849-8871, <https://doi.org/10.5194/acp-18-8849-2018>, 2018.

1398 Lu, D., Xu, J., Yang, D., and Zhao, J.: Spatio-temporal variation and influence factors
1399 of PM_{2.5} concentrations in China from 1998 to 2014, *Atmospheric Pollution*
1400 *Research*, 8, 1151-1159, <https://doi.org/10.1016/j.apr.2017.05.005>, 2017.

1401 Lyons, W. A.: The climatology and prediction of the Chicago lake breeze, *Journal of*

1402 Applied Meteorology and Climatology, 11, 1259-1270, 1972.

1403 Lyons, W. A. and Olsson, L. E.: Detailed mesometeorological studies of air pollution
1404 dispersion in the Chicago lake breeze, Monthly Weather Review, 101, 387-403,
1405 1973.

1406 Lyons, W. A., Pielke, R. A., Tremback, C. J., Walko, R. L., Moon, D. A., and Keen, C.
1407 S.: MODELING IMPACTS OF MESOSCALE VERTICAL MOTIONS UPON
1408 COASTAL ZONE AIR-POLLUTION DISPERSION, Atmospheric Environment,
1409 29, 283-301, [https://doi.org/10.1016/1352-2310\(94\)00217-9](https://doi.org/10.1016/1352-2310(94)00217-9), 1995.

1410 Makar, P. A., Zhang, J., Gong, W., Stroud, C., Sills, D., Hayden, K. L., Brook, J., Levy,
1411 I., Mihele, C., Moran, M. D., Tarasick, D. W., He, H., and Plummer, D.: Mass
1412 tracking for chemical analysis: the causes of ozone formation in southern Ontario
1413 during BAQS-Met 2007, Atmospheric Chemistry and Physics, 10, 11151-11173,
1414 <https://doi.org/10.5194/acp-10-11151-2010>, 2010.

1415 Miao, Y., Liu, S., Chen, B., Zhang, B., Wang, S., and Li, S.: Simulating urban flow and
1416 dispersion in Beijing by coupling a CFD model with the WRF model, Advances in
1417 Atmospheric Sciences, 30, 1663-1678, [https://doi.org/10.1007/s00376-013-2234-](https://doi.org/10.1007/s00376-013-2234-9)
1418 [9](https://doi.org/10.1007/s00376-013-2234-9), 2013.

1419 Miao, Y., Guo, J., Liu, S., Liu, H., Li, Z., Zhang, W., and Zhai, P.: Classification of
1420 summertime synoptic patterns in Beijing and their associations with boundary
1421 layer structure affecting aerosol pollution, Atmospheric Chemistry and Physics, 17,
1422 3097-3110, <https://doi.org/10.5194/acp-17-3097-2017>, 2017.

1423 Mlawer, E. J., Taubman, S. J., Brown, P. D., Iacono, M. J., and Clough, S. A.: Radiative
1424 transfer for inhomogeneous atmospheres: RRTM, a validated correlated-k model
1425 for the longwave, Journal of Geophysical Research-Atmospheres, 102, 16663-
1426 16682, <https://doi.org/10.1029/97jd00237>, 1997.

1427 Monks, P. S., Archibald, A. T., Colette, A., Cooper, O., Coyle, M., Derwent, R., Fowler,
1428 D., Granier, C., Law, K. S., Mills, G. E., Stevenson, D. S., Tarasova, O., Thouret,
1429 V., von Schneidemesser, E., Sommariva, R., Wild, O., and Williams, M. L.:
1430 Tropospheric ozone and its precursors from the urban to the global scale from air
1431 quality to short-lived climate forcer, Atmospheric Chemistry and Physics, 15,

1432 8889-8973, <https://doi.org/10.5194/acp-15-8889-2015>, 2015.

1433 Morrison, H., Thompson, G., and Tatarskii, V.: Impact of Cloud Microphysics on the
1434 Development of Trailing Stratiform Precipitation in a Simulated Squall Line:
1435 Comparison of One- and Two-Moment Schemes, *Monthly Weather Review*, 137,
1436 991-1007, <https://doi.org/10.1175/2008mwr2556.1>, 2009.

1437 NCEP: NCEP FNL operational model global tropospheric analyses, continuing from
1438 July 1999, Research Data Archive at the National Center for Atmospheric
1439 Research, Computational and Information Systems Laboratory [data set],
1440 <https://doi.org/https://doi.org/10.5065/D6M043C6>, 2000.

1441 Peng, J., Huang, Y., Liu, T., Jiang, L., Xu, Z., Xing, W., Feng, X., and De Maeyer, P.:
1442 Atmospheric nitrogen pollution in urban agglomeration and its impact on alpine
1443 lake-case study of Tianchi Lake, *Science of the Total Environment*, 688, 312-323,
1444 <https://doi.org/10.1016/j.scitotenv.2019.06.202>, 2019.

1445 Sills, D. M. L., Brook, J. R., Levy, I., Makar, P. A., Zhang, J., and Taylor, P. A.: Lake
1446 breezes in the southern Great Lakes region and their influence during BAQS-Met
1447 2007, *Atmospheric Chemistry and Physics*, 11, 7955-7973,
1448 <https://doi.org/10.5194/acp-11-7955-2011>, 2011.

1449 Steiner, A. L., Mermelstein, D., Cheng, S. J., Twine, T. E., and Oliphant, A.: Observed
1450 Impact of Atmospheric Aerosols on the Surface Energy Budget, *Earth Interactions*,
1451 17, <https://doi.org/10.1175/2013ei000523.1>, 2013.

1452 Stull, R. B.: *An Introduction to Boundary Layer Meteorology*, Springer Nether
1453 lands, 1988.

1454 Unger, N., Menon, S., Koch, D. M., and Shindell, D. T.: Impacts of aerosol-cloud
1455 interactions on past and future changes in tropospheric composition, *Atmospheric
1456 Chemistry and Physics*, 9, 4115-4129, <https://doi.org/10.5194/acp-9-4115-2009>,
1457 2009.

1458 Wang, F., Wang, Y., and Gao, M.: Impact of lake-atmosphere exchange on summertime
1459 ozone in the Lake Taihu region, *Atmospheric Environment*, 300,
1460 <https://doi.org/10.1016/j.atmosenv.2023.119664>, 2023.

1461 Wang, Y., Ying, Q., Hu, J., and Zhang, H.: Spatial and temporal variations of six criteria

1462 air pollutants in 31 provincial capital cities in China during 2013-2014,
1463 Environment International, 73, 413-422,
1464 <https://doi.org/10.1016/j.envint.2014.08.016>, 2014.

1465 Wang, Y., Gao, Y., Qin, H., Huang, J., Liu, C., Hu, C., Wang, W., Liu, S., and Lee, X.:
1466 Spatiotemporal Characteristics of Lake Breezes over Lake Taihu, China, Journal
1467 of Applied Meteorology and Climatology, 56, 2053-2065,
1468 <https://doi.org/10.1175/jamc-d-16-0220.1>, 2017.

1469 Wei, J., Li, Z., Pinker, R. T., Wang, J., Sun, L., Xue, W., Li, R., and Cribb, M.:
1470 Himawari-8-derived diurnal variations in ground-level PM_{2.5} pollution across
1471 China using the fast space-time Light Gradient Boosting Machine (LightGBM),
1472 Atmospheric Chemistry and Physics, 21, 7863-7880, [https://doi.org/10.5194/acp-](https://doi.org/10.5194/acp-21-7863-2021)
1473 [21-7863-2021](https://doi.org/10.5194/acp-21-7863-2021), 2021.

1474 Wentworth, G. R., Murphy, J. G., and Sills, D. M. L.: Impact of lake breezes on ozone
1475 and nitrogen oxides in the Greater Toronto Area, Atmospheric Environment, 109,
1476 52-60, <https://doi.org/10.1016/j.atmosenv.2015.03.002>, 2015.

1477 Wiedinmyer, C., Akagi, S. K., Yokelson, R. J., Emmons, L. K., Al-Saadi, J. A., Orlando,
1478 J. J., and Soja, A. J.: The Fire INventory from NCAR (FINN): a high resolution
1479 global model to estimate the emissions from open burning, Geoscientific Model
1480 Development, 4, 625-641, <https://doi.org/10.5194/gmd-4-625-2011>, 2011.

1481 Wild, O., Zhu, X., and Prather, M. J.: Fast-j: Accurate simulation of in- and below-
1482 cloud photolysis in tropospheric chemical models, Journal of Atmospheric
1483 Chemistry, 37, 245-282, <https://doi.org/10.1023/a:1006415919030>, 2000.

1484 WRAP – Western Regional Air Partnership: 2002 Fire Emission Inventory for the
1485 WRAP Region – Phase II, Project No.178-6, available at:
1486 <http://www.wrapair.org/forums/fejftasks/FEJFtask7PhaseII.html> (last access: 30
1487 September 2021), 2005.

1488 Yang, Y., Ruan, Z., Wang, X., Yang, Y., Mason, T. G., Lin, H., and Tian, L.: Short-term
1489 and long-term exposures to fine particulate matter constituents and health: A
1490 systematic review and meta-analysis, Environmental Pollution, 247, 874-882,
1491 <https://doi.org/10.1016/j.envpol.2018.12.060>, 2019.

1492 Yang, Z. N., Du, Q. Y., Yang, Q. K., Zhao, C., Li, G. D. Z., Xia, Z. H., Xu, M. Y., Yuan,
1493 R. M., Li, Y. B., Xia, K. H., Gu, J., and Feng, J. W.: Modeling urban pollutant
1494 transport at multiple resolutions: impacts of turbulent mixing, *Atmospheric*
1495 *Chemistry and Physics*, 25, 8831-8857, <https://doi.org/10.5194/acp-25-8831-2025>,
1496 2025.

1497 Yue, X., Ma, N. L., Sonne, C., Guan, R., Lam, S. S., Le, Q. V., Chen, X., Yang, Y., Gu,
1498 H., Rinklebe, J., and Peng, W.: Mitigation of indoor air pollution: A review of
1499 recent advances in adsorption materials and catalytic oxidation, *Journal of*
1500 *Hazardous Materials*, 405, <https://doi.org/10.1016/j.jhazmat.2020.124138>, 2021.

1501 Zaveri, R. A. and Peters, L. K.: A new lumped structure photochemical mechanism for
1502 large-scale applications, *Journal of Geophysical Research-Atmospheres*, 104,
1503 30387-30415, <https://doi.org/10.1029/1999jd900876>, 1999.

1504 Zhang, H., Wang, Y., Hu, J., Ying, Q., and Hu, X.-M.: Relationships between
1505 meteorological parameters and criteria air pollutants in three megacities in China,
1506 *Environmental Research*, 140, 242-254,
1507 <https://doi.org/10.1016/j.envres.2015.04.004>, 2015a.

1508 Zhang, L., Zhu, B., Gao, J., and Kang, H.: Impact of Taihu Lake on city ozone in the
1509 Yangtze River Delta, *Advances in Atmospheric Sciences*, 34, 226-234,
1510 <https://doi.org/10.1007/s00376-016-6099-6>, 2017.

1511 Zhang, M., Zhao, C., Yang, Y., Du, Q., Shen, Y., Lin, S., Gu, D., Su, W., and Liu, C.:
1512 Modeling sensitivities of BVOCs to different versions of MEGAN emission
1513 schemes in WRF-Chem (v3.6) and its impacts over eastern China, *Geoscientific*
1514 *Model Development*, 14, 6155-6175, <https://doi.org/10.5194/gmd-14-6155-2021>,
1515 2021.

1516 Zhang, R., Wang, G., Guo, S., Zarnora, M. L., Ying, Q., Lin, Y., Wang, W., Hu, M., and
1517 Wang, Y.: Formation of Urban Fine Particulate Matter, *Chemical Reviews*, 115,
1518 3803-3855, <https://doi.org/10.1021/acs.chemrev.5b00067>, 2015b.

1519 Zhang, R., Jing, J., Tao, J., Hsu, S. C., Wang, G., Cao, J., Lee, C. S. L., Zhu, L., Chen,
1520 Z., Zhao, Y., and Shen, Z.: Chemical characterization and source apportionment of
1521 PM_{2.5} in Beijing: seasonal perspective, *Atmospheric Chemistry and Physics*, 13,

1522 7053-7074, <https://doi.org/10.5194/acp-13-7053-2013>, 2013.

1523 Zhang, X. Y., Wang, Y. Q., Niu, T., Zhang, X. C., Gong, S. L., Zhang, Y. M., and Sun,
1524 J. Y.: Atmospheric aerosol compositions in China: spatial/temporal variability,
1525 chemical signature, regional haze distribution and comparisons with global
1526 aerosols, *Atmospheric Chemistry and Physics*, 12, 779-799,
1527 <https://doi.org/10.5194/acp-12-779-2012>, 2012.

1528 Zhao, C., Liu, X., Leung, L. R., and Hagos, S.: Radiative impact of mineral dust on
1529 monsoon precipitation variability over West Africa, *Atmospheric Chemistry and*
1530 *Physics*, 11, 1879-1893, <https://doi.org/10.5194/acp-11-1879-2011>, 2011.

1531 Zhao, C., Leung, L. R., Easter, R., Hand, J., and Avise, J.: Characterization of speciated
1532 aerosol direct radiative forcing over California, *Journal of Geophysical Research-*
1533 *Atmospheres*, 118, 2372-2388, <https://doi.org/10.1029/2012jd018364>, 2013a.

1534 Zhao, C., Chen, S., Leung, L. R., Qian, Y., Kok, J. F., Zaveri, R. A., and Huang, J.:
1535 Uncertainty in modeling dust mass balance and radiative forcing from size
1536 parameterization, *Atmospheric Chemistry and Physics*, 13, 10733-10753,
1537 <https://doi.org/10.5194/acp-13-10733-2013>, 2013b.

1538 Zhao, C., Hu, Z., Qian, Y., Leung, L. R., Huang, J., Huang, M., Jin, J., Flanner, M. G.,
1539 Zhang, R., Wang, H., Yan, H., Lu, Z., and Streets, D. G.: Simulating black carbon
1540 and dust and their radiative forcing in seasonal snow: a case study over North
1541 China with field campaign measurements, *Atmospheric Chemistry and Physics*, 14,
1542 11475-11491, <https://doi.org/10.5194/acp-14-11475-2014>, 2014.

1543 Zhao, C., Huang, M., Fast, J. D., Berg, L. K., Qian, Y., Guenther, A., Gu, D.,
1544 Shrivastava, M., Liu, Y., Walters, S., Pfister, G., Jin, J., Shilling, J. E., and Warneke,
1545 C.: Sensitivity of biogenic volatile organic compounds to land surface
1546 parameterizations and vegetation distributions in California, *Geoscientific Model*
1547 *Development*, 9, 1959-1976, <https://doi.org/10.5194/gmd-9-1959-2016>, 2016.

1548 Zheng, B., Tong, D., Li, M., Liu, F., Hong, C., Geng, G., Li, H., Li, X., Peng, L., Qi, J.,
1549 Yan, L., Zhang, Y., Zhao, H., Zheng, Y., He, K., and Zhang, Q.: Trends in China's
1550 anthropogenic emissions since 2010 as the consequence of clean air actions,
1551 *Atmospheric Chemistry and Physics*, 18, 14095-14111,

1552 <https://doi.org/10.5194/acp-18-14095-2018>, 2018.

1553

1554

1555

1556

1557

1558

1559

1560

1561

1562

1563

1564

1565

1566

1567

1568

1569

1570

1571

1572

1573

1574

1575

1576

1577

1578

1579

1580

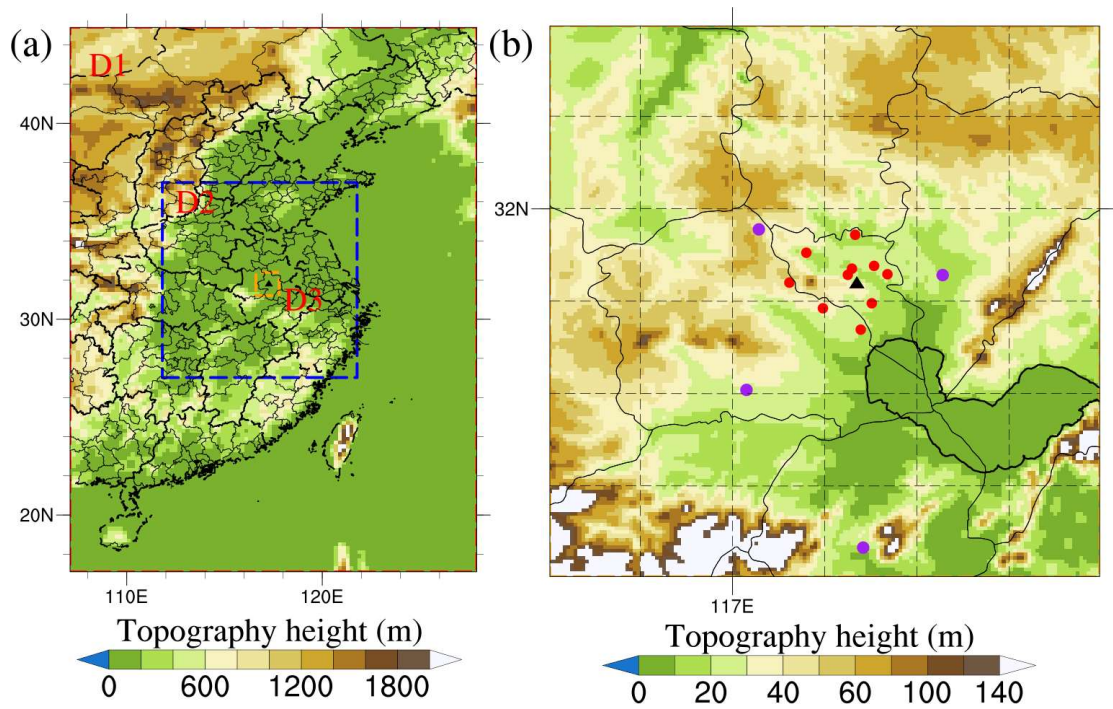
1581

1582

Table 1 WRF-Chem model configuration

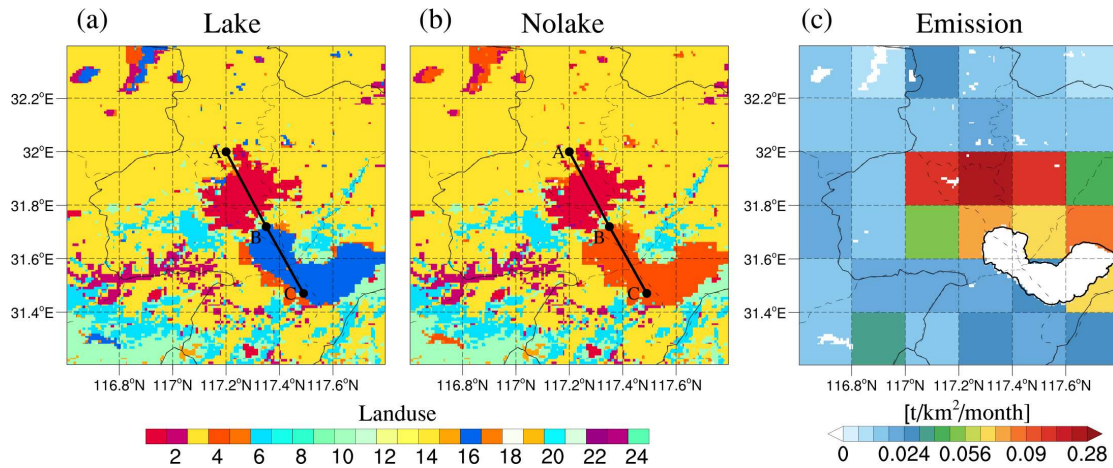
Horizontal resolution	25, 5, and 1 km
Domain size (grid cells)	140 × 105, 250 × 250, and 150 × 150
Simulation period	5 to 21 March 2019
Gas-phase chemistry scheme	CBMZ mechanism
Radiation scheme	Fast-J
PBL scheme	Yonsei University (YSU) scheme
Microphysics scheme	Morrison two-moment scheme
Land surface scheme	Noah land surface scheme
Cumulus scheme	Kain-Fritsch (25 km grid only)
Surface layer scheme	Revised MM5 Monin-Obukhov scheme
Longwave radiation scheme	RRTMG scheme
Shortwave radiation scheme	RRTMG scheme

1583
1584
1585
1586
1587
1588
1589
1590
1591
1592
1593
1594
1595
1596
1597
1598
1599
1600
1601
1602
1603



1604
 1605
 1606
 1607
 1608
 1609
 1610
 1611
 1612
 1613
 1614
 1615
 1616
 1617
 1618
 1619
 1620
 1621
 1622
 1623
 1624
 1625

Figure 1. (a) The three domains used in the WRF-Chem simulations and the terrain height (m) of each domain. Domain one (D1) has a horizontal grid spacing of 25 km, domain 2 (D2) 5 km, and domain 3 (D3) 1 km; (b) The spatial distribution of the terrain height (m) in D3. The solid black triangle indicates the location of Hefei, the solid dots triangles indicate MEP monitoring sites, and the purple solid dots indicate AWSs locations.



1626

1627 **Figure 2.** The spatial distribution of land use types in the (a) Lake experiment and (b)
 1628 Nolake experiment across the study area, with detailed descriptions of the legend and
 1629 land cover classes provided in Table S1 in the Supplement. (c) The spatial distribution
 1630 of PM_{2.5} emissions in both the Lake and Nolake experiments averaged over the entire
 1631 day throughout the study area. The black line segments (AB and BC) in panels (a) and
 1632 (b) represent transects selected for subsequent detailed analyses, traversing both urban
 1633 and lake regions to capture the spatial characteristics of lake-urban interactions.

1634

1635

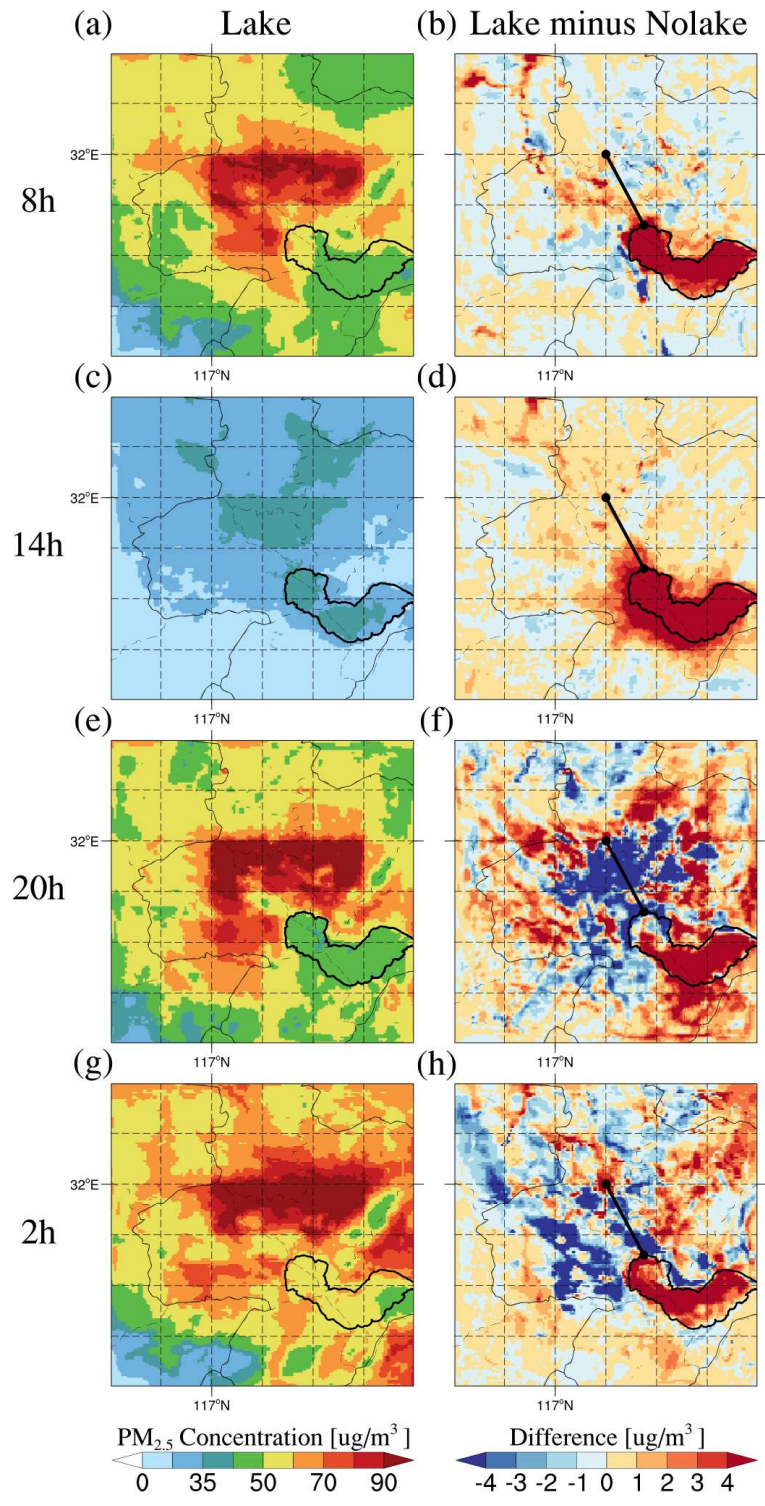
1636

1637

1638

1639

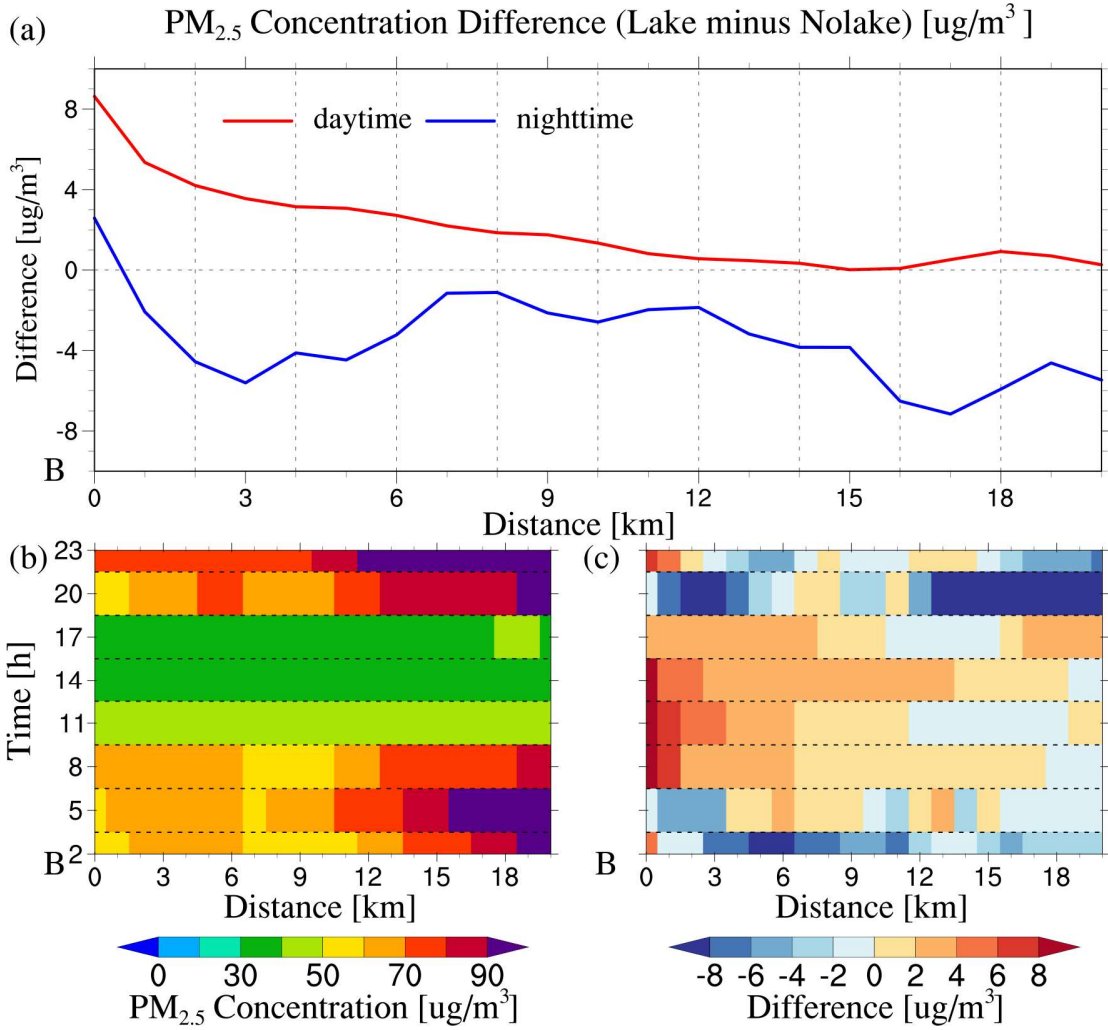
1640



1641

1642 **Figure 3.** The spatial distribution of PM_{2.5} near-surface concentrations in the (a, c,
 1643 e, g) Lake experiment and (b, d, f, h) the differences between Lake and Nolake
 1644 experiments (Lake minus Nolake) at 08:00, 14:00, 20:00, and 02:00 local time (LT)
 1645 across the study area, averaged over 10-20 March 2019. Note that the line segments
 1646 shown in panels (b, d, f, h) correspond to the AB transect marked in Figure 2.

1647



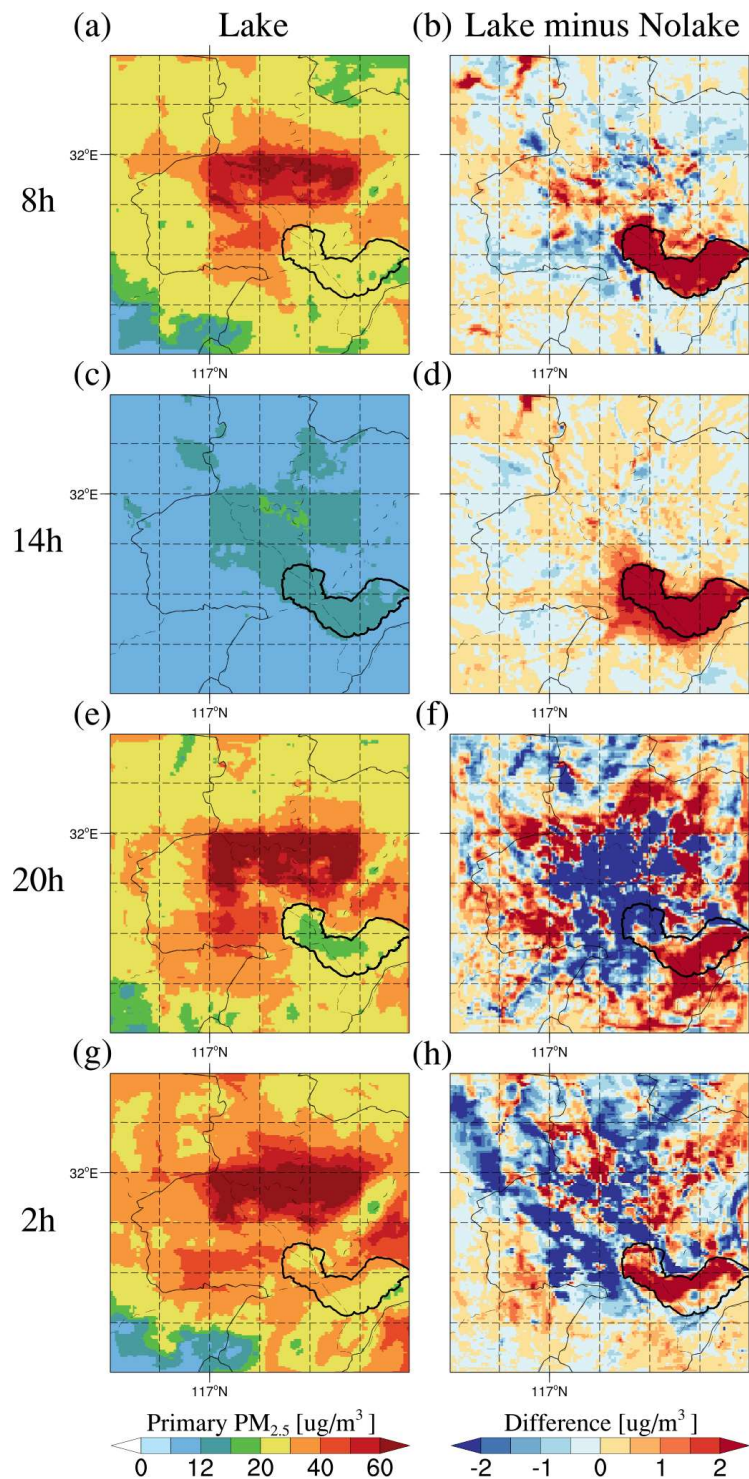
1648

1649 **Figure 4.** Diurnal variation of PM_{2.5} near-surface concentration along the path. (a)
 1650 Average PM_{2.5} concentration differences (Lake minus Nolake) during daytime (the
 1651 average of 08:00, 11:00, 14:00, and 17:00 LT, red line) and nighttime (the average of
 1652 20:00, 23:00, 02:00, and 05:00 LT, blue line), averaged over 10-20 March 2019, as a
 1653 function of distance from point B toward A, as marked in Figure S2 and S3. (b) Diurnal
 1654 variation of PM_{2.5} concentration with distance in the Lake experiments. (c) Diurnal
 1655 variation of PM_{2.5} concentration differences between Lake and Nolake experiments
 1656 (Lake minus Nolake) with distance. The x-axis represents the distance from point B
 1657 along the transect, the y-axis in (a) represents the concentration difference, and the y-
 1658 axis in (b) and (c) represents the local time.

1659

1660

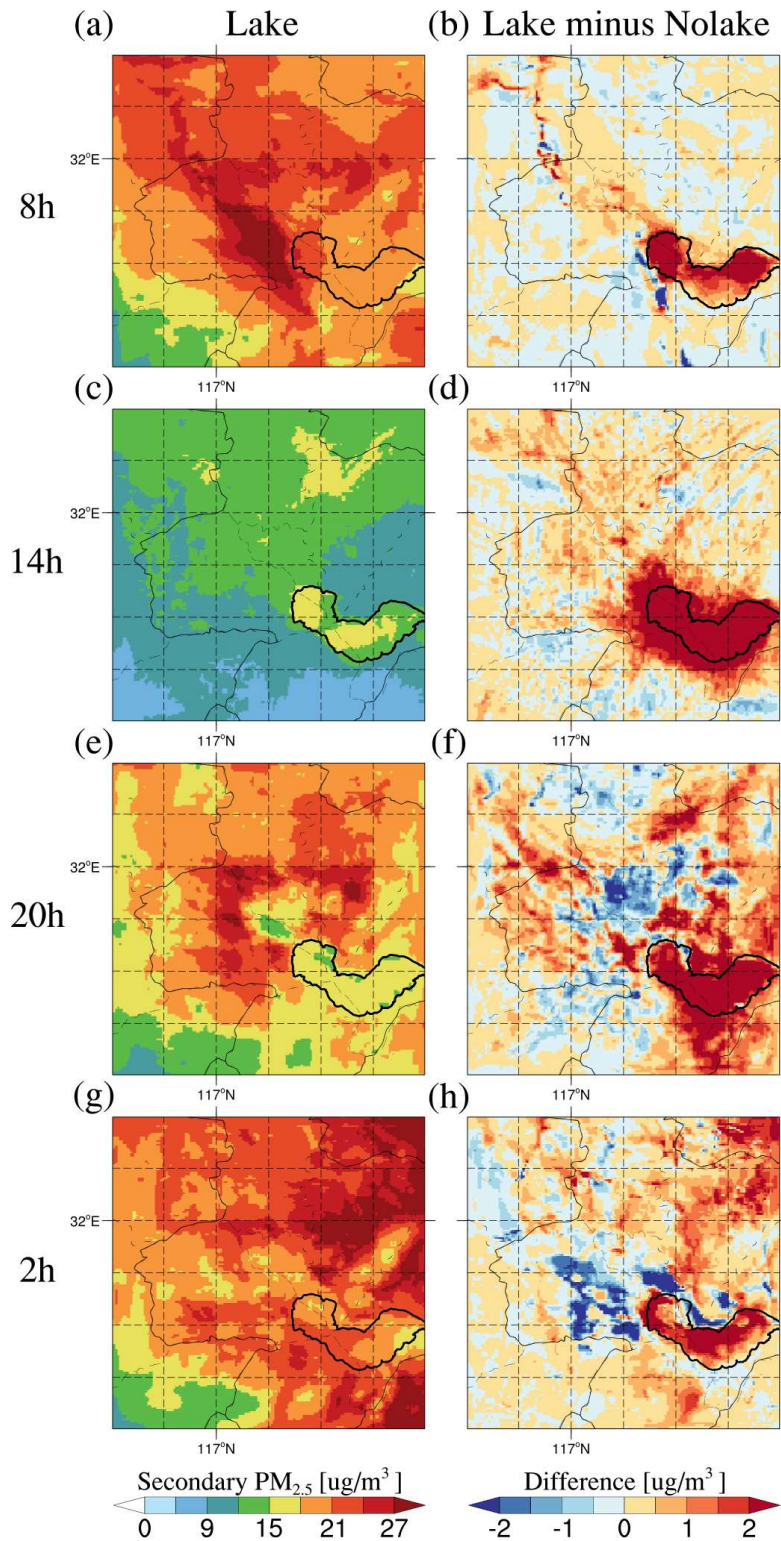
1661



1662

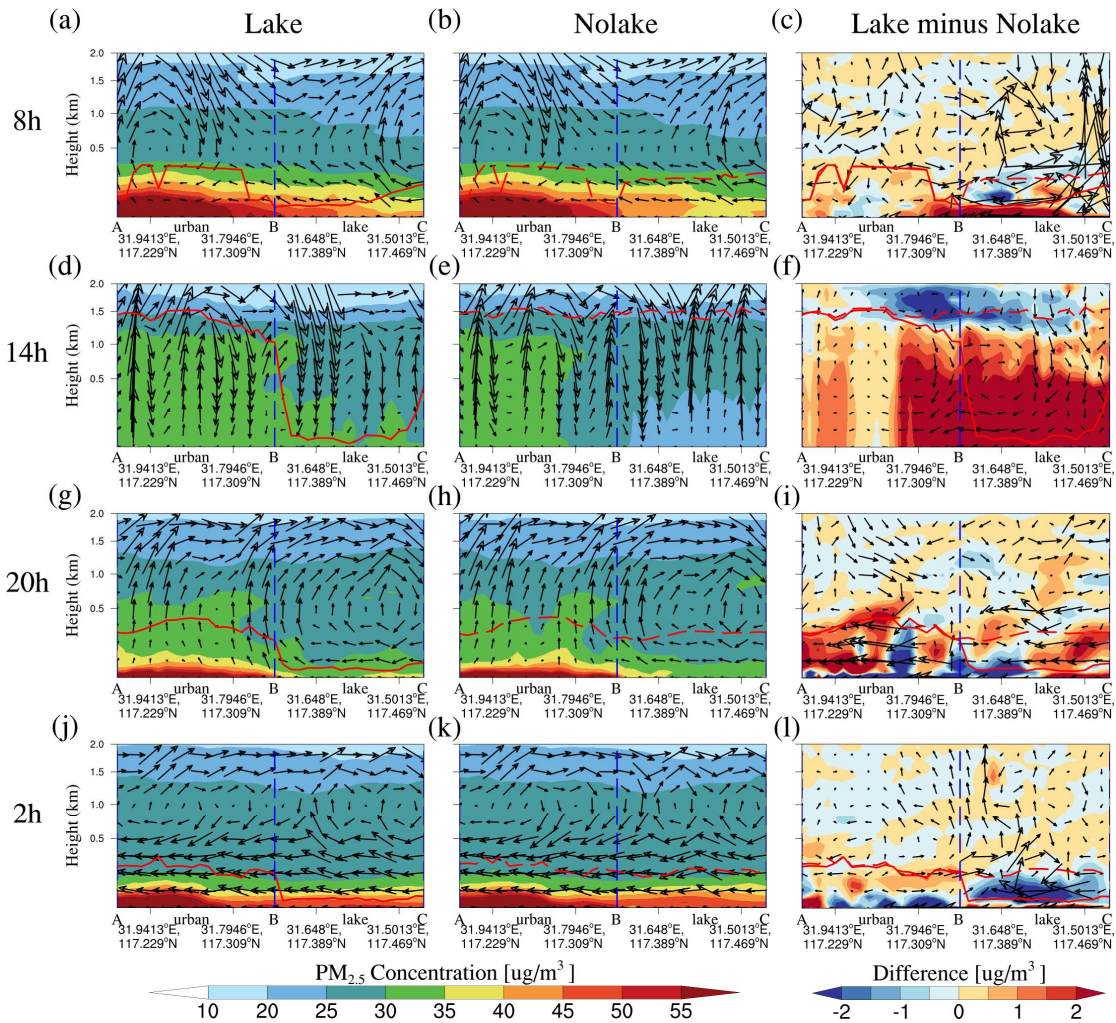
1663 **Figure 5A.** The spatial distribution of primary $PM_{2.5}$ near-surface concentrations (sum
 1664 of black carbon (BC), organic carbon (OC), and other inorganics (OIN)) in the (a, c,
 1665 e, g) Lake experiment and (b, d, f, h) the differences between Lake and Nolake
 1666 experiments (Lake minus Nolake) at 08:00, 14:00, 20:00, and 02:00 LT across the study
 1667 area, averaged over 10-20 March 2019.

1668



1669

1670 **Figure 5B.** The spatial distribution of secondary PM_{2.5} near-surface concentrations
 1671 (sum of sulfate (SO₄²⁻), nitrate(NO₃⁻), and ammonium (NH₄⁺)) in the (a、c、e、g) Lake
 1672 experiment and (b、d、f、h) the differences between Lake and Nolake experiments
 1673 (Lake minus Nolake) at 08:00, 14:00, 20:00, and 02:00 LT across the study area,
 1674 averaged over 10-20 March 2019.

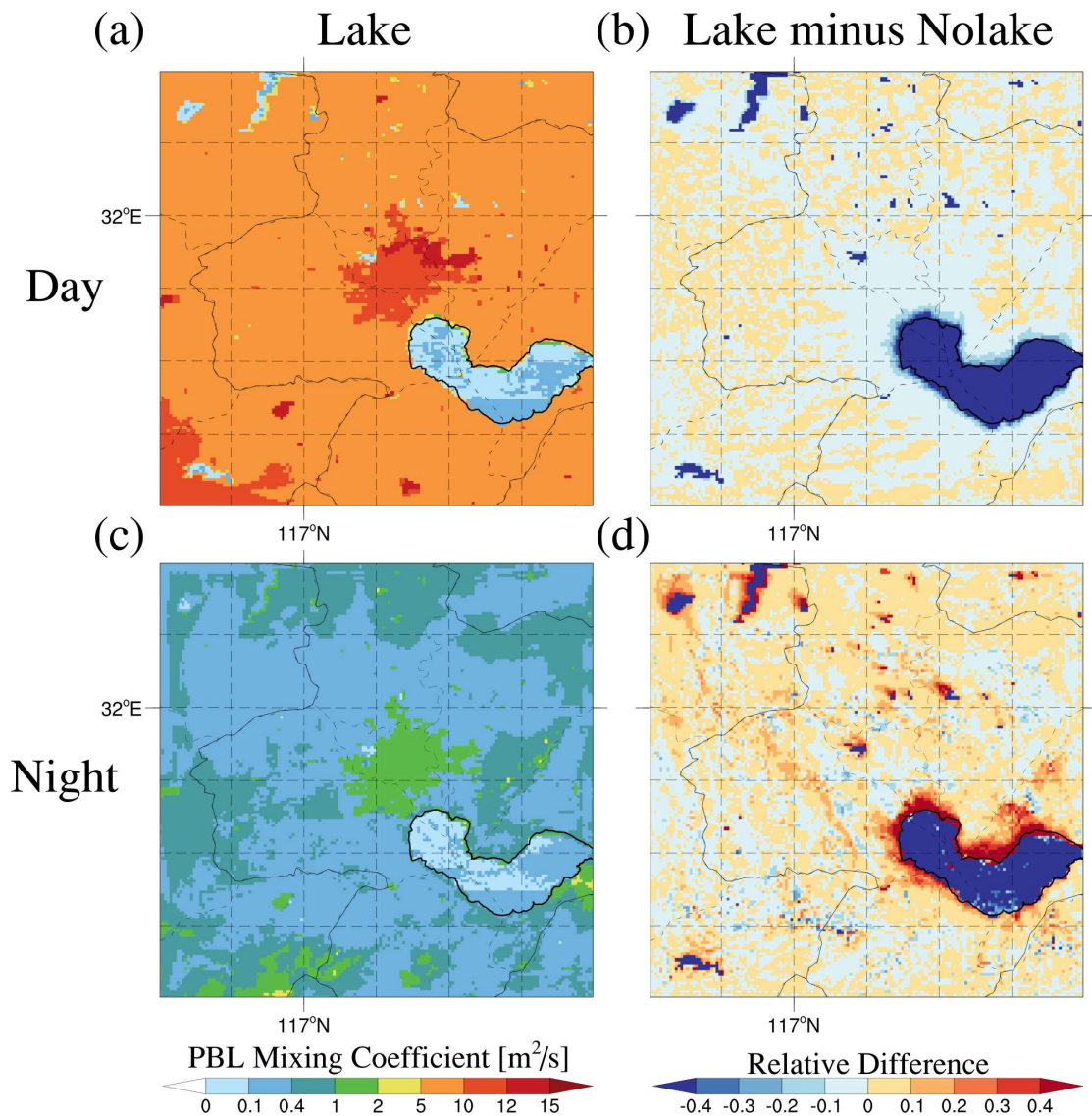


1675

1676 **Figure 6.** The vertical cross-section of PM_{2.5} concentration and wind vectors along the
 1677 key path AC (indicated in Figure 2) for the (a、d、g、j) Lake experiment, (b、e、h、
 1678 k) Nolake experiment, and (c、f、i、l) their differences (Lake minus Nolake) at 08:00,
 1679 14:00, 20:00, and 02:00 LT, averaged over 10-20 March 2019. The shaded contours
 1680 represent PM_{2.5} concentrations or their differences between the two experiments at each
 1681 altitude. The black vector arrows indicate the superimposed vertical wind field
 1682 (including horizontal and vertical wind components), with the vertical vector being
 1683 multiplied by 50 for visibility. The red solid line represents the planetary boundary layer
 1684 height (PBLH) in the Lake experiment, and the red dashed line represents the planetary
 1685 boundary layer height in the Nolake experiment. The blue dashed line represents the
 1686 lake-land boundary.

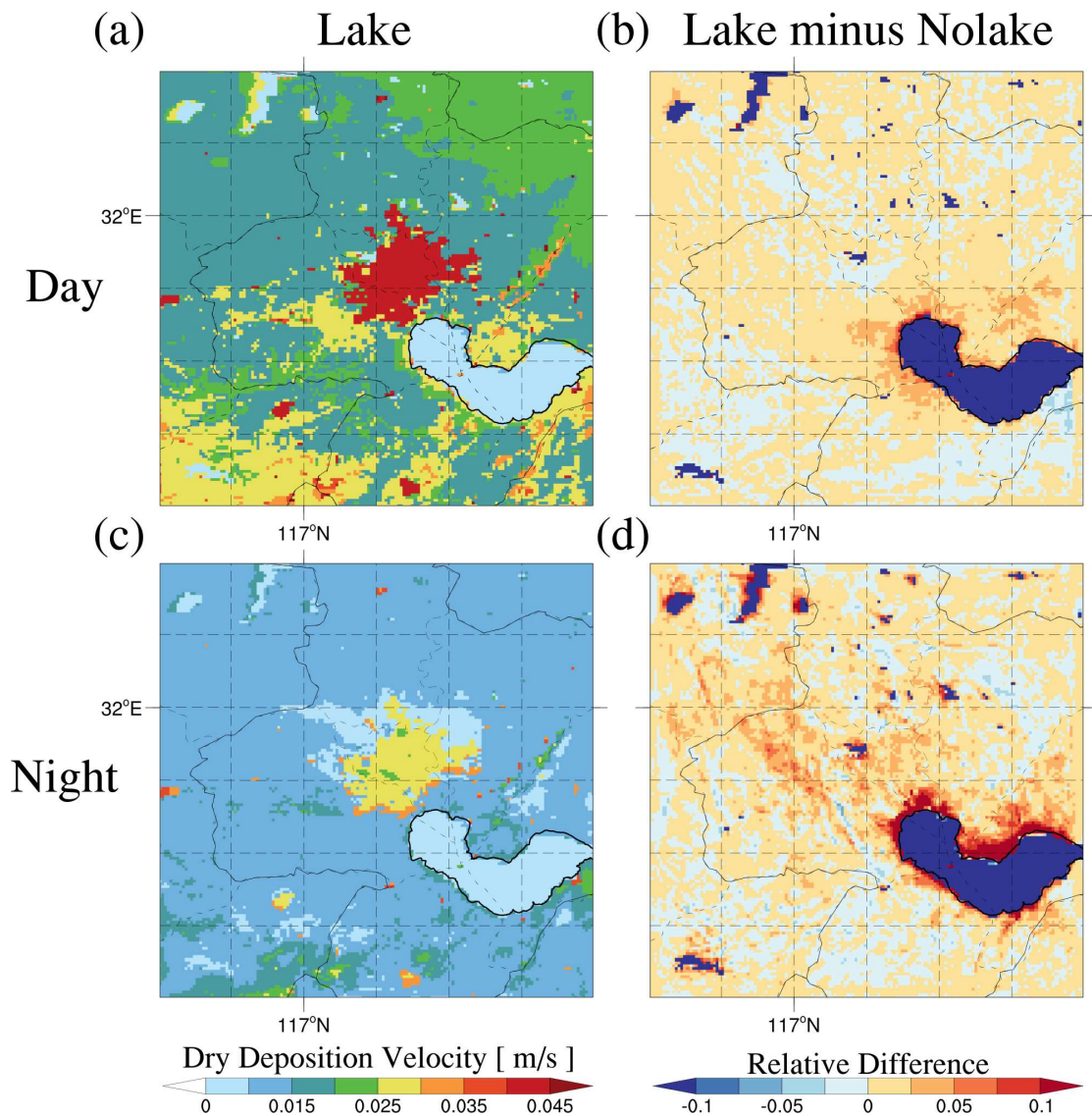
1687

1688



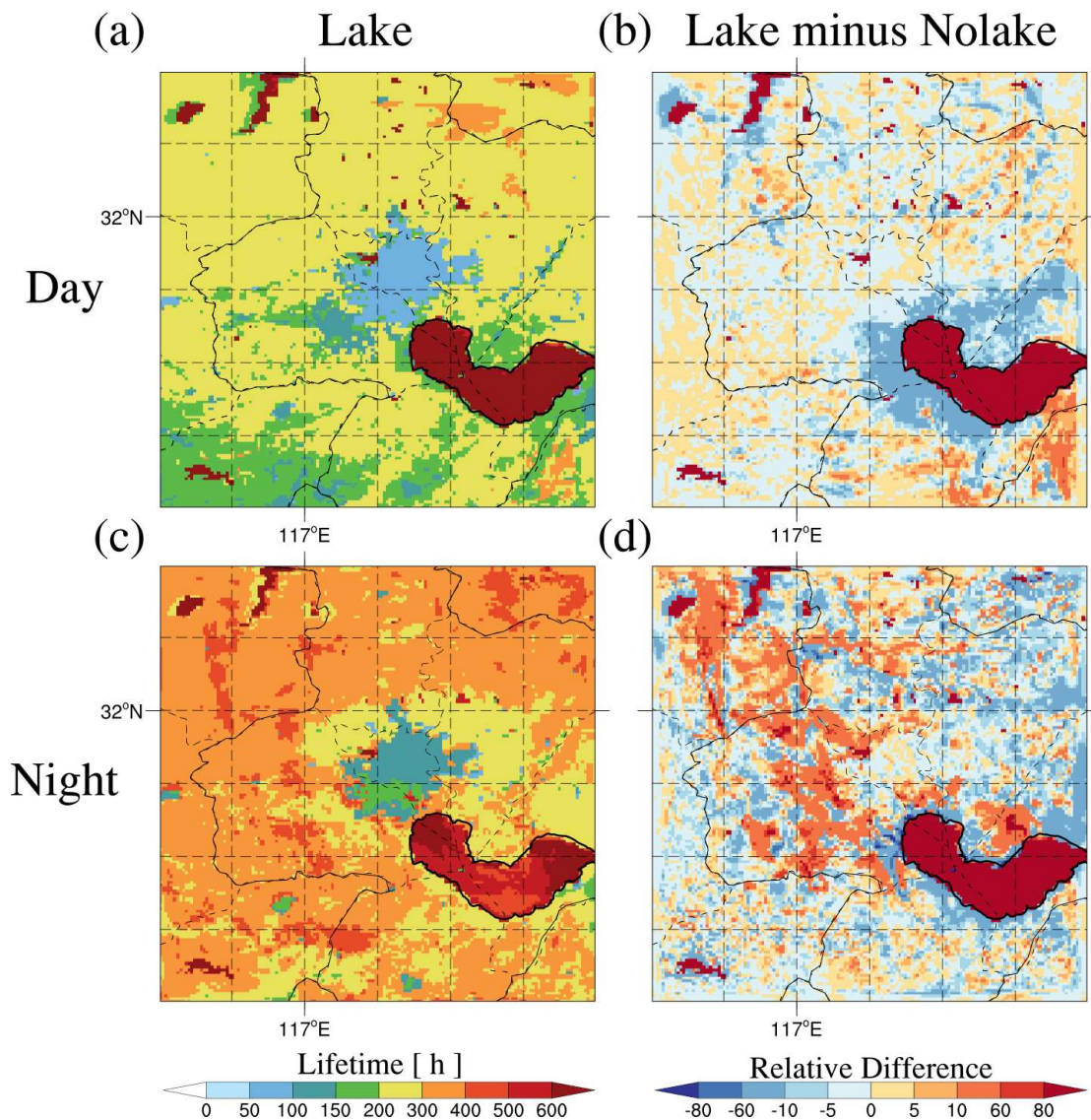
1689
 1690 **Figure 7.** The spatial distribution of planetary boundary layer (PBL) mixing
 1691 coefficients averaged during (a, b) daytime (08:00, 11:00, 14:00, and 17:00 LT,
 1692 averaged over 10-20 March 2019) and (c, d) nighttime (20:00, 23:00, 02:00, and 05:00
 1693 LT, averaged over 10-20 March 2019) for the (a, c) Lake experiment and (b, d) relative
 1694 differences ((Lake - Nolake)/Lake) across the study area.

1695
 1696
 1697
 1698
 1699
 1700
 1701



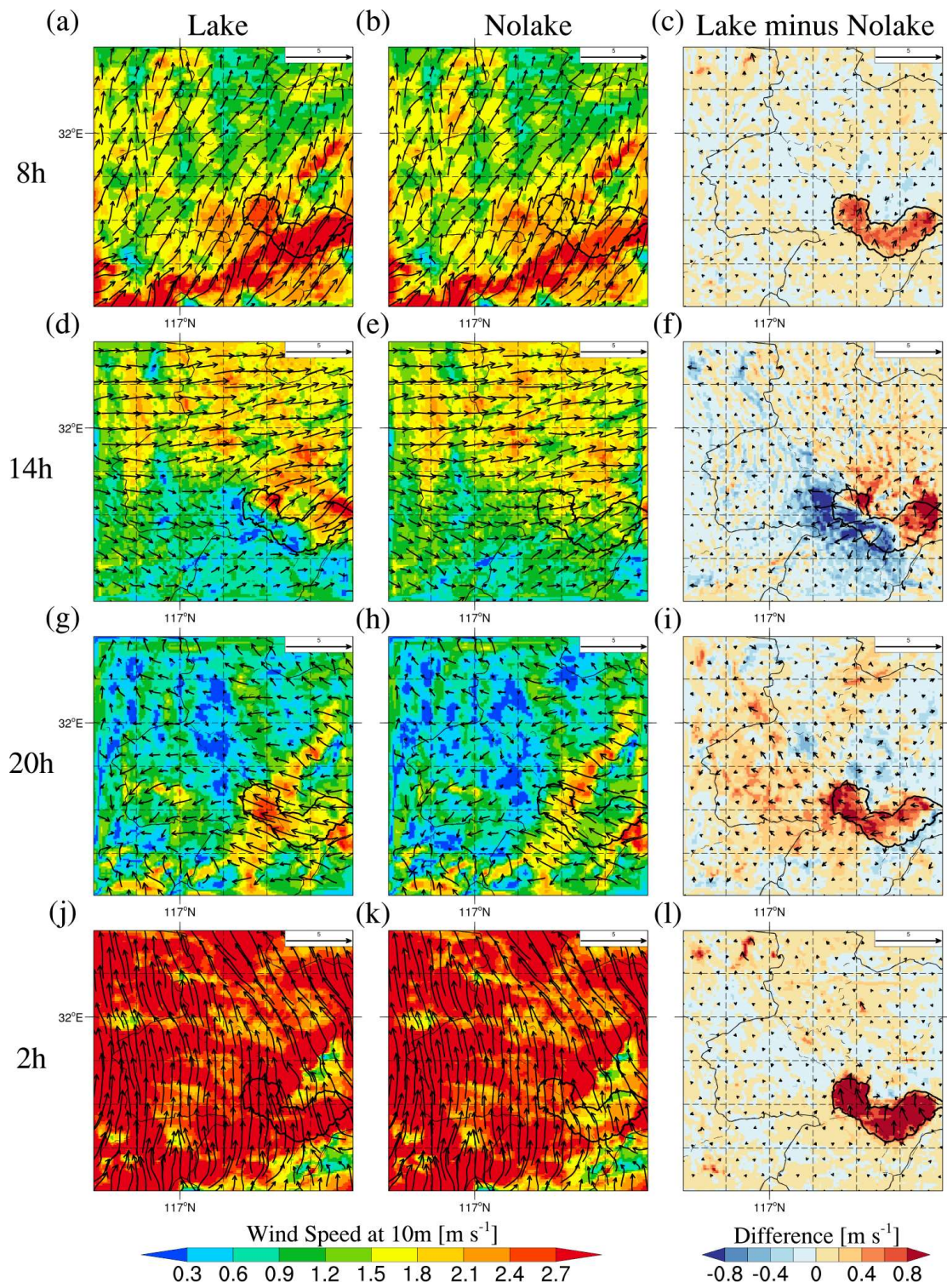
1702
 1703 **Figure 8.** The spatial distribution of dry deposition velocity averaged during (a, b)
 1704 daytime (08:00, 11:00, 14:00, and 17:00 LT, averaged over 10-20 March 2019) and (c,
 1705 d) nighttime (20:00, 23:00, 02:00, and 05:00 LT, averaged over 10-20 March 2019) for
 1706 the (a, c) Lake experiment and (b, d) relative differences $((\text{Lake} - \text{Nolake})/\text{Lake})$ across
 1707 the study area.

1708
 1709
 1710
 1711
 1712
 1713
 1714



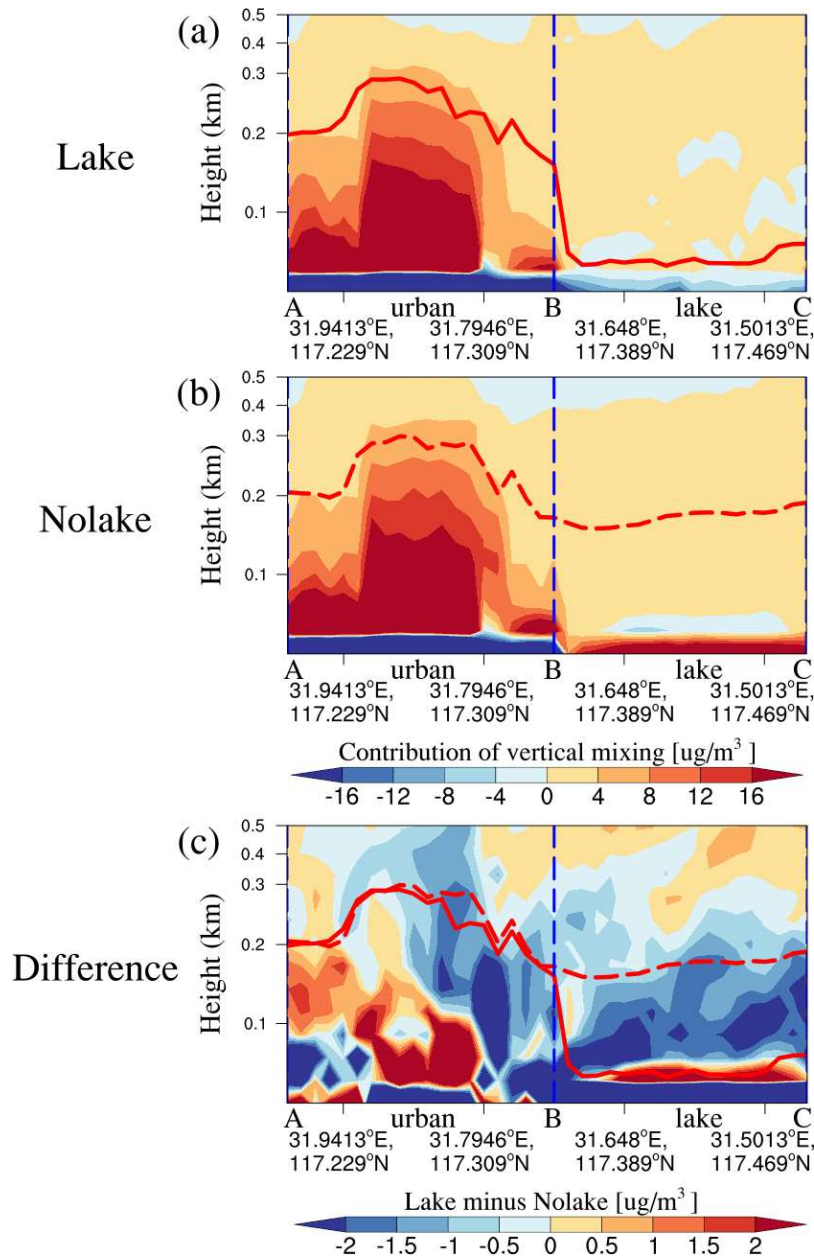
1715
 1716 **Figure 9.** The spatial distribution of the lifetime averaged during (a, b) daytime (08:00,
 1717 11:00, 14:00, and 17:00 LT, averaged over 10-20 March 2019) and (c, d) nighttime
 1718 (20:00, 23:00, 02:00, and 05:00 LT, averaged over 10-20 March 2019) for the (a, c)
 1719 Lake experiment and (b, d) relative differences $((\text{Lake} - \text{Nolake})/\text{Lake})$ across the study
 1720 area. The PM_{2.5} lifetime is calculated by dividing the PM_{2.5} column concentration by
 1721 the dry deposition flux.

1722
 1723
 1724
 1725
 1726
 1727



1728
 1729
 1730
 1731
 1732
 1733

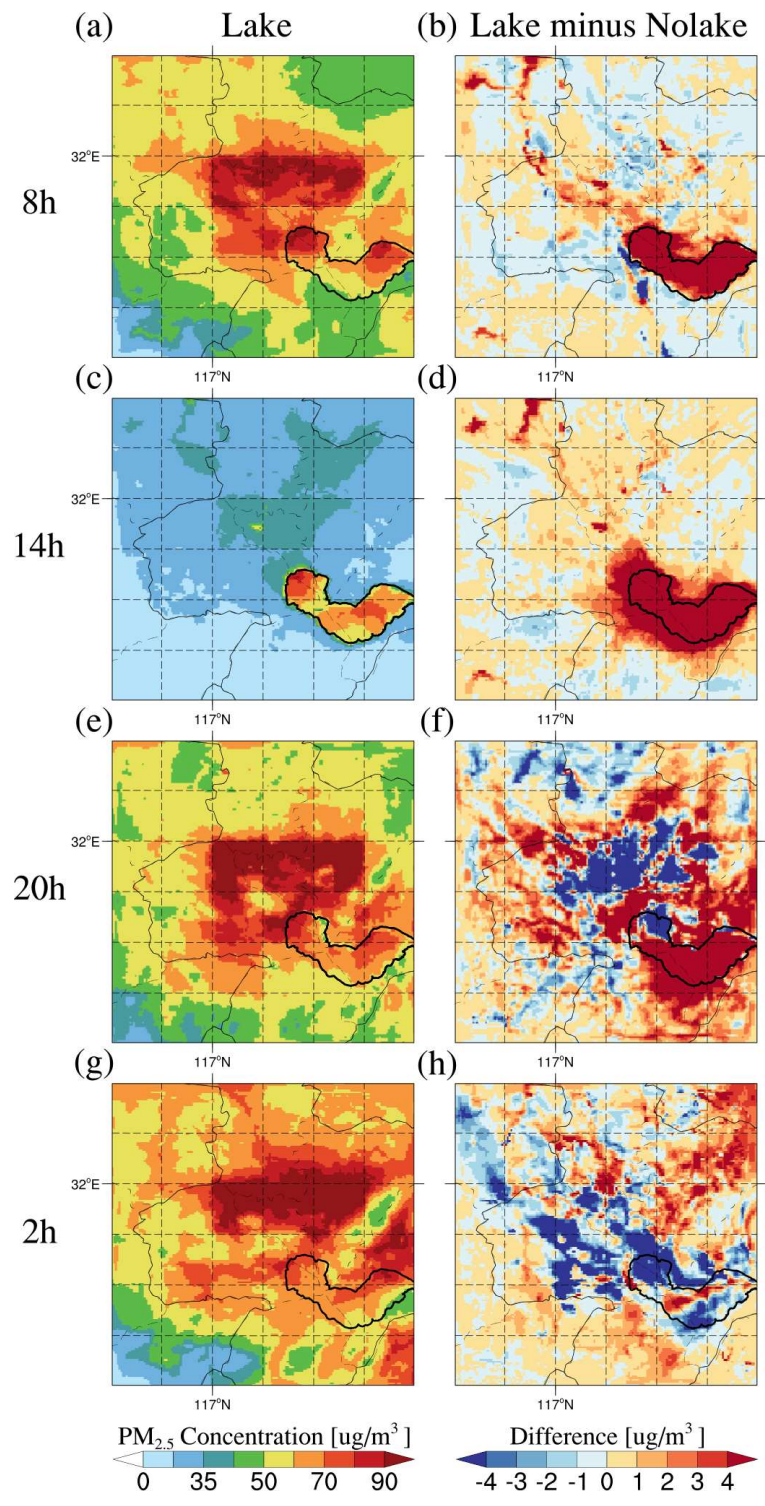
Figure 10. The spatial distribution of 10-m wind speed in the (a、d、g、j) Lake experiment, (b、e、h、k) Nolake experiment, and (c、f、i、l) their differences (Lake minus Nolake) at 08:00, 14:00, 20:00, and 02:00 LT across the study area, averaged over 10-20 March 2019.



1734

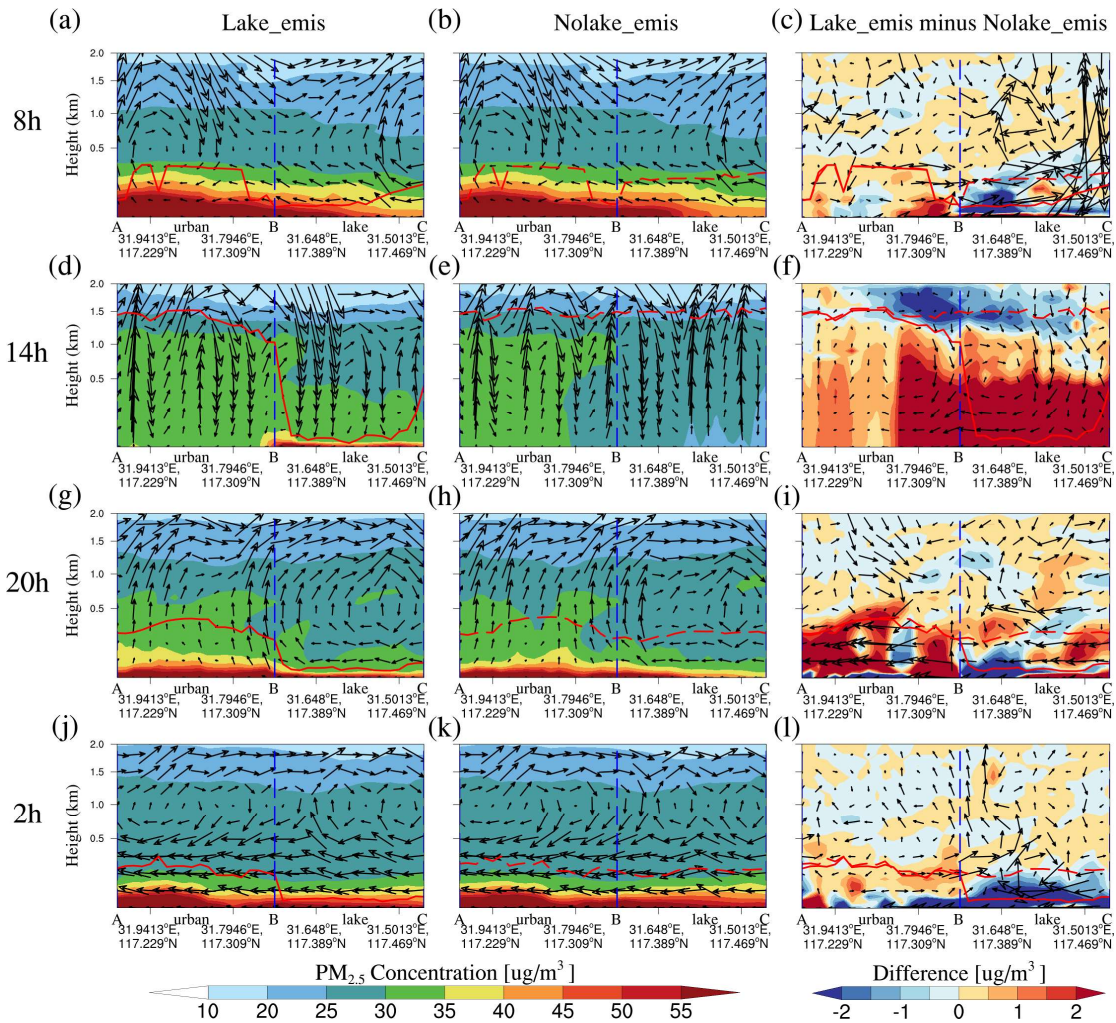
1735 **Figure 11.** The vertical cross-section of PBL mixing process contributions to $PM_{2.5}$
 1736 concentrations along the key path AC (indicated in Figure 2) for the (a) Lake
 1737 experiment, (b) Nolake experiment, and (c) their differences (Lake minus Nolake)
 1738 during nighttime, averaged over 10-20 March 2019. The shaded contours represent the
 1739 contribution of PBL mixing processes to surface $PM_{2.5}$ concentrations or their
 1740 differences between the two experiments at each altitude. The red solid line represents
 1741 the PBLH in the Lake experiment, and the red dashed line represents the PBLH in the
 1742 Nolake experiment. The blue dashed line represents the lake-land boundary.

1743



1744
 1745
 1746
 1747
 1748
 1749

Figure 12. The spatial distribution of $PM_{2.5}$ near-surface concentrations in the (a, c, e, g) Lake_emis experiment and (b, d, f, h) the differences between Lake_emis and Nolake_emis experiments (Lake_emis minus Nolake_emis) at 08:00, 14:00, 20:00, and 02:00 LT across the study area, averaged over 10-20 March 2019.



1750

1751 **Figure 13.** The vertical cross-section of $PM_{2.5}$ concentration and wind vectors along
 1752 the key path AC (indicated in Figure 2) for the (a, d, g, j) Lake_emis experiment, (b,
 1753 e, h, k) Nolake_emis experiment, and (c, f, i, l) their differences (Lake_emis minus
 1754 Nolake_emis) at 08:00, 14:00, 20:00, and 02:00 LT, averaged over 10-20 March 2019.
 1755 The shaded contours represent $PM_{2.5}$ concentrations or their differences between the
 1756 two experiments at each altitude. The black vector arrows indicate the superimposed
 1757 vertical wind field (including horizontal and vertical wind components), with the
 1758 vertical wind vector being multiplied by 50 for visibility. The red solid line represents
 1759 the planetary boundary layer height (PBLH) in the Lake experiment, and the red dashed
 1760 line represents the planetary boundary layer height in the Nolake experiment. The blue
 1761 dashed line represents the lake-land boundary.

1762